Antigen-scaffolds drive preferential expansion of functional genetically engineered CAR and TCR T cells

Kristoffer Haurum Johansen[*,1,(0000-0002-7711-9451)], Keerthana Ramanathan[*,1,(0000-0001-7245-9169)], Carlos Rodriguez-Pardo[1], Anne Kargaard Gjelstrup[1], Hólmfridur Rósa Halldórsdóttir[1], Lasse Frank Voss[1], Siri Tvingsholm[1], Laura Stentoft Grand[1], Edoardo Dionisio[1], Alberte H. Skriver[1], Louise Pii Frederiksen[1], Mette Bjørnson[1], Marcus Svensson-Frej[1], Maria Ormhøj[1], Sine Reker Hadrup[1,†]

[1] T cells and cancer, Experimental and Translational Immunology Section, Department for Health Technology, Technical University of Denmark, 2800 Kongens Lyngby, Denmark

[*]These authors have contributed equally.

[†]Lead author: Email: Sirha@dtu.dk

Summary

The engineering of autologous T cells to express chimeric antigen receptors (CARs) can induce profound clinical responses in haematological malignancies, while T cell receptor-engineered T (TCR T) cells have led to durable responses in clinical trials for solid tumours. However, clinical manufacturing of engineered T cells is resource-intensive and often yields highly differentiated, exhausted effector T cells. To circumvent this, we have developed an antigen-scaffold (Ag-scaffold) technology to preferentially expand genetically engineered T cells. Such Ag-scaffolds present cognate antigen together with stimulatory factors such as cytokines. By providing a specific and receptor-engaging stimulation to CAR/TCR T cells, the expanded product is highly enriched for engineered T cells with a favourable proliferative and efficacious phenotype.

We expanded TCR T cells with Ag-scaffolds presenting peptide MHC (pMHC), and anti-CD19 CAR T cells with Ag-scaffolds presenting CD19 antigen. By applying cognate pMHC Ag-scaffolds, we achieved >80% antigen-specific T cells (83.62%±9.2%) after 14 days of culture with a distinct cytotoxic, proliferative phenotypical profile. Ag-scaffold expansion enhanced initial TCR and CAR cytotoxicity; sustained control was observed after repeated rechallenges of CAR T cells. *In vivo*, Ag-scaffold-expanded CRISPR/Cas9-engineered anti-CD19 CAR T also showed complete tumour eradication in a B-cell lymphoma xenograft model with a low dose of CAR T cells, which was not achieved using IL2/7/15 expansion.

Keywords

CRISPR, Cas9, T-cell engineering, TCR T cells, CAR T cells, Chimeric antigen receptor, Interleukin-2, TCR complex, Artificial antigen-presenting scaffolds.

37 **Introduction**

38 T-cell engineering aimed at modifying the T-cell specificity using synthetic antigen receptors, such
39 as chimeric antigen receptors (CARs) or recombinant T-cell receptors (TCRs), has demonstrated
40 significant efficacy in treating malignancies[1]. CAR-engineered T cells (CAR T cells) can induce
41 durable responses in hematologic malignancies; however, they have been less successful in treating
42 solid cancers[2]. With the approval of the first FDA TCR-engineered T-cell therapy, afamitresgene
43 autoleucel (Tecelra®), targeting MAGE-A4/HLA-A*02:01^{+} synovial sarcomas, TCR therapies have
44 shown efficacy in treating solid malignancies[2].

45 Traditionally, synthetic antigen receptors are introduced into T cells *ex vivo* by lentiviral transduction,
46 followed by expansion with a cytokine cocktail of IL2, IL7, and IL15[1,3]. However, in recent years,
47 pre-clinical and clinical studies have investigated nonviral introduction of CARs and TCRs into the
48 endogenous TCR alpha constant locus (TRAC) by CRISPR/Cas9-mediated knockin (KI), allowing
49 for endogenous control of the synthetic antigen receptor expression whilst simultaneously replacing
50 the endogenous TCR[4,5]. Pre-clinical evidence supports that expressing the CAR/TCR under the
51 regulation of the endogenous TCR promoter enhances the efficacy of the anti-tumour effect of the T
52 cells[5,6].

53 Although engineered T-cell therapies have proven successful in cancer immunotherapy, their efficacy
54 is governed by the phenotype and functional properties of the final adoptive cell therapy product
55 (ACT). Long-term follow-up of the CD19 CAR T cell-treated patients shows that, despite the initial
56 complete response, a significant proportion of patients experience relapse due to poor cytotoxicity
57 and persistence of the CAR T cells[7–9]. The antigen stimulus and the cytokines present during the *ex*
58 *vivo* expansion greatly influence T-cell phenotype and functional properties. Early differentiated T-
59 cell populations, such as stem-cell memory (T_{SCM}) and central memory (T_{CM}), have demonstrated
60 enhanced tumour control in pre-clinical studies and early clinical trials due to their high self-renewal
61 capacity[7,10,11]. On the contrary, the more differentiated T-cell phenotypes, such as T_{EMRA} and T_{reg}
62 cells, are associated with reduced therapeutic efficacy due to their poor persistence and
63 functionality[12]. The conventional *ex vivo* expansion protocol involves initial stimulation with anti-
64 CD3/anti-CD28 antibodies, followed by expansion in IL2-supplemented media[13,14]. However, the
65 unspecific polyclonal activation driven by anti-CD3/CD28 and IL2 leads to a highly differentiated T-
66 cell phenotype, resulting in a suboptimal ACT product[15]. Consequently, subsequent studies have
67 identified that the regulation of early differentiated phenotypes depends on other cytokines that share
68 the common gamma chain, namely IL7, IL15, and IL21[3,16, 17].

69 Additionally, antigen-mediated activation and co-stimulation using autologous (monocyte-derived
70 dendritic cells; moDC) or artificial antigen-presenting platforms in combination with cytokines have
71 shown some pre-clinical promise in improving the ACT product[14,18]. While antigen-specific T-cell
72 expansion using patient-derived dendritic cells (DCs) has shown clinical efficacy, challenges remain
73 in the complex manufacturing process. The recent advances in generating off-the-shelf, customisable,
74 and biocompatible nano- and micro-materials have facilitated the development of novel antigen-
75 presenting platforms that can provide T cells with the optimal signals to support the phenotype and
76 functional characteristics of a desirable ACT product[18,19].

77 Here, we apply a linear streptavidin-coated dextran scaffold that can be customised by coupling the
78 respective biotinylated CAR antigen or pMHC complex, together with cytokines (Ag-scaffold), to
79 specifically activate and expand TCR or CAR T cells for ACT[20]. We applied IL-2/IL-21 on the Ag-
80 scaffold based on earlier optimisation showing superiority of this cytokine combination in antigen-
81 specific T-cell expansion[20] and the concept that Ag-scaffold-mediated antigen engagement fosters
82 localised paracrine cytokine signalling. We tested the Ag-scaffold technology in T cells engineered
83 with CRISPR/Cas9 KI or lentiviral vectors and compared their expansion and phenotype extensively
84 with conventional expansion protocols. We demonstrate that Ag-scaffold-mediated expansion of
85 engineered T cells yields an enriched T-cell product characterised by high self-renewal, enhanced
86 proliferation, and increased cytotoxicity.

87 ## Results

88 ### Ag-scaffolds specifically enrich for genetically engineered TCR and CAR T cells

89 Non-viral CRISPR/Cas9-mediated KI of TCRs and CARs in the TRAC locus is relatively low (10-
90 30%) (**Figure S1A-C**) (gRNA and HDRT sequences in Table S1). To test whether we could
91 specifically expand T cells with successful KI, we established a method using Ag-scaffolds presenting
92 the pMHC antigen for TCRs (TCR Ag-scaffolds) or CAR antigen for CARs (CAR Ag-scaffolds)
93 together with IL2 and IL21, as shown to be the optimal Ag-scaffold composition in earlier work[21].
94 We knocked in TCRs or CARs 2 days after T-cell activation and expanded the TCR or CAR T cells
95 with Ag-scaffolds added to the culture on days 4, 7, and 10, followed by analysis on day 14 (**Figures**
96 **1A-B**). To test whether we could use TCR Ag-scaffolds to specifically expand genetically engineered
97 TCR T cells, we knocked in the alpha and beta chains of the NY-ESO-1-specific
98 (SLLMWITQC/HLA-A*02:01) 1G4 TCR in the TRAC locus and compared expansion of T cells
99 with soluble IL2/IL7/IL15 to Ag-scaffold expansion using SLLMWITQC/HLA-A*02:01/IL2/IL21-

coated dextran scaffolds (TCR Ag-scaffolds). Using TCR Ag-scaffolds, CRISPR/Cas9 NY-ESO-1-specific TCR T cells were highly enriched (83.62%±9.2%) compared to T cells only expanded with cytokines (18.5%±9.2%) (**Figures 1C-E**). Further, the total number of antigen-specific TCR T cells was increased in the TCR Ag-scaffold-expanded population, with a 160-fold (SD=35.08) expansion of the TCR T cells after Ag-scaffold feeding, compared to 39-fold (SD=4.48) expansion in the cytokine controls over the same timeframe (**Figures 1F-H**). Interestingly, we did not observe specific expansion until after the second feed on day 5 post-KI **(Figures 1D, H**), suggesting that initial activation drove proliferation in the first days of culture.

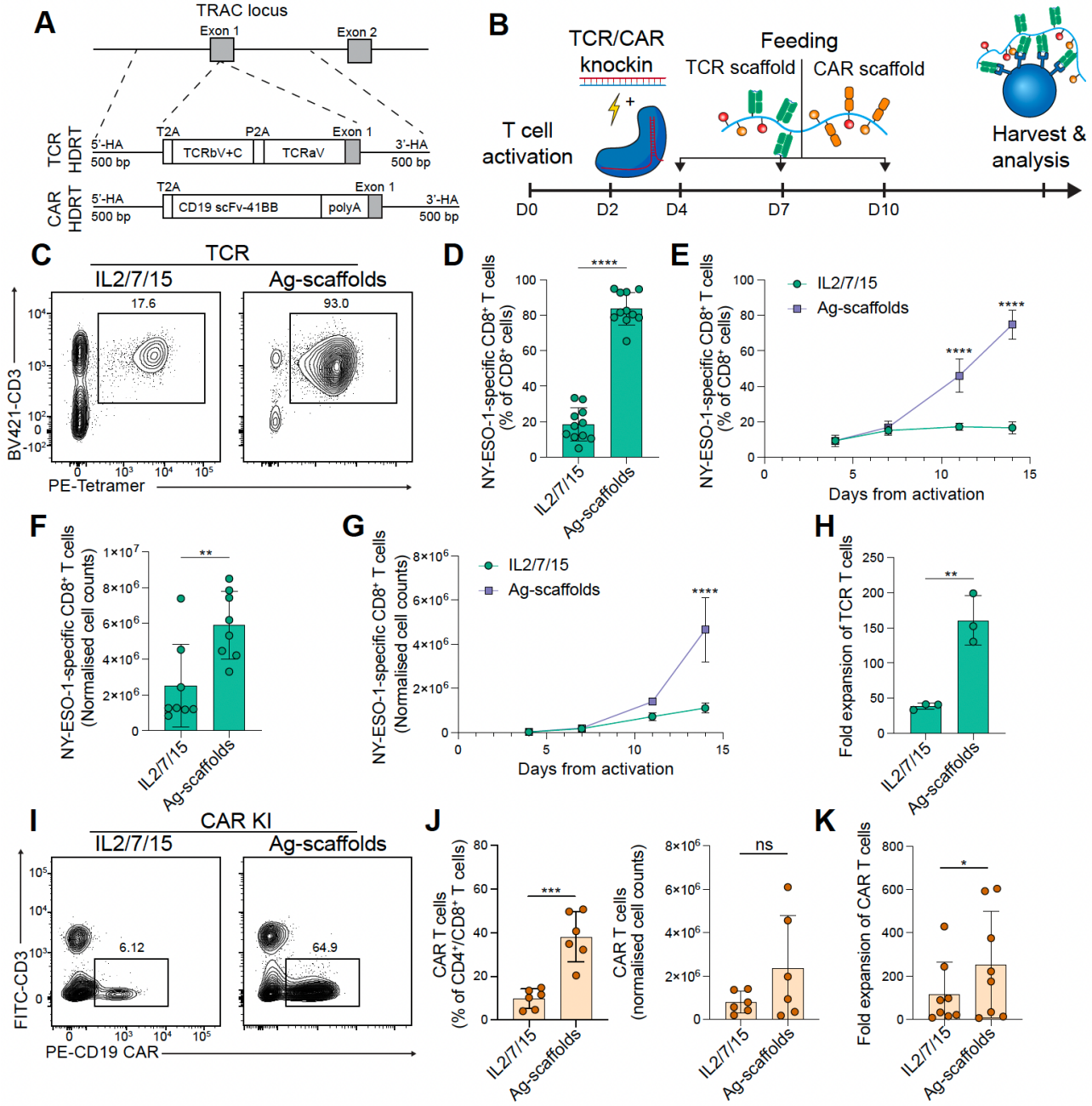

Figure 1. Antigen scaffold-mediated expansion of TCR- and CAR T cells greatly enriches KI TCR and CAR T cells. (**A**) Schematic representation of TCR and CAR KI homology-directed repair template (HDRT) with 500 bp homology arms (HA) targeting exon 1 of the TRAC locus. (**B**) A timeline illustrating the activation, KI, and Ag-scaffold feeding of engineered T cells. (**C**) Representative flow cytometry plots of NY-ESO-1-specific CRISPR/Cas9 1G4 TCR T cells after expansion with either IL2/IL7/IL15 or Ag-scaffolds. (**D-E**) Comparison of tetramer-positive (Tet^+) percentages of $CD8^+$ T cells at day 14 (**D**; n = 11 biological replicates per group), and (**E**) at different timepoints during expansion (n = 3 biological replicates per group). (**F-H**) Comparison of number of total specific cells at day 14 (**F**; n = 8 biological replicates per group), and over time (**G**) as well as the fold expansion from day 4 normalised to an initial count of 1 million total cells (**G, H**; n = 3 biological replicates per group). (**I**) Representative flow cytometry plots of CAR T cells expanded with IL2/7/15 or Ag-scaffolds. (**J**) Comparison of tetramer-positive (Tet^+) percentages of $CD4^+/CD8^+$ T cells (n = 6 biological replicates per group) and cell counts (n = 6 biological replicates per group) following Ag-scaffold or IL2/IL7/IL15 expansion, with (**K**) fold expansion calculated from day 4 normalised to an initial count of $1x10^6$ total cells. Data in panels (**D-F**) represent pooled results from 3-4 experiments, (**H**) and (**K**) represent pooled results from 2 experiments presented as mean ± SD, with each dot indicating one PBMC sample post-KI. Statistical significance determined by ratio-paired t-test: *P < 0.05, **P < 0.01, ***P < 0.001, ****P < 0.0001.

Similarly to TCR KI, CAR KI in the TRAC locus exhibits limited KI efficiency (**Figure S1C**). We therefore generated CAR Ag-scaffolds using biotinylated CD19 antigen together with IL2 and IL21 to expand anti-CD19 CAR T cells. The CD19 CAR was knocked into T cells using the protocol described above. The KI CAR T cells were fed with CAR Ag-scaffolds every 3-4 days from day 4 post-activation as described above. The scaffolds were tested with 10 µM, 25 µM, and 50 µM per million T cells, and the results demonstrate a specific expansion effect using the CAR Ag-scaffold, which saturates at 25 µM/10^6 cells (**Figure S1D**). Hence, we chose to continue with 25 uM of Ag-scaffolds per million T cells for CAR Ag-scaffolds. CAR Ag-scaffold expansion of CRISPR/Cas9 KI CAR T cells yielded a product with >35% CAR T cells (38.1%±11.5%) (**Figure 1I-J).** Furthermore, the CAR Ag-scaffold expansion resulted in a superior 400-fold expansion of CAR T cells, compared to 190-fold using free soluble cytokines (**Figure 1K**).

Ag-scaffolds drive a distinct transcriptomic T cell phenotype with high proliferative capacity

To evaluate the effects of Ag-scaffold expansion on the phenotype and functional capacity of lentiviral or CRISPR/Cas9-engineered CAR T or TCR T cells, we compared the use of Ag-scaffolds to several established expansion protocols. Specifically, we tested two conventional cytokine cocktails commonly used for expanding engineered T cells: IL2 (200 IU/mL) + IL7 (5 ng/mL) + IL15

142 (5 ng/mL), and IL7 (5 ng/mL) + IL15 (5 ng/mL). Additionally, we evaluated IL2 (20 IU/mL) + IL21
143 (30 ng/mL) in solution to directly compare the effects of soluble versus scaffold-bound cytokines
144 **(Figures S2A-D).** We proceeded with in-depth comparisons of the scaffold-expanded T cells to the
145 cytokine cocktail (IL2 (200 IU/ml) + IL7 (5 ng/mL) + IL15 (5 ng/mL)) for further phenotypic and
146 extensive functional analysis.

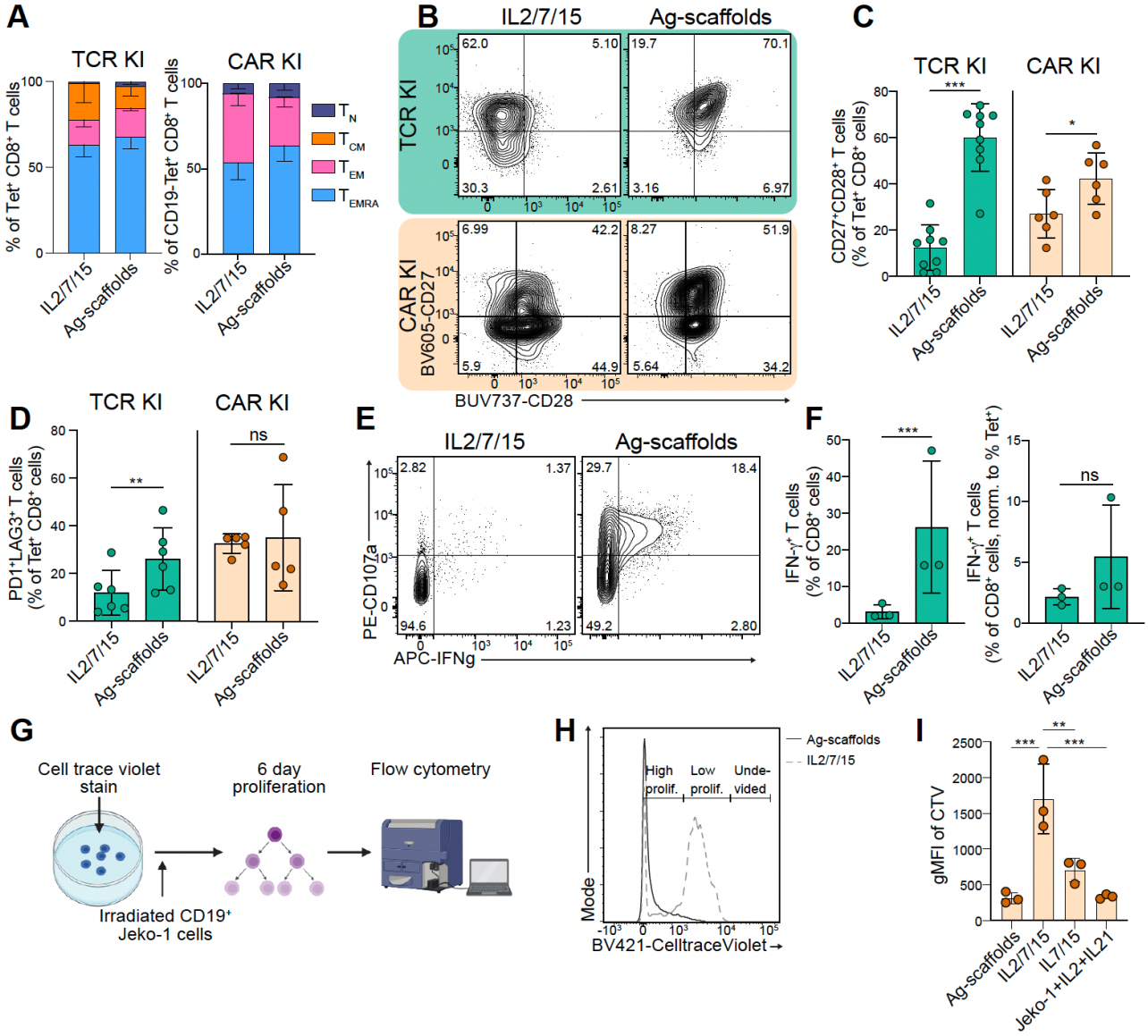

147

148 **Figure 2. Ag-scaffold-mediated expansion of CRISPR/Cas9 T cells yields phenotypically distinct cells**
149 **with superior cytotoxicity.** (**A-F**) Phenotypic and functional analysis of CRISPR/Cas9 TCR/CAR KI T cells
150 expanded using CAR/TCR Ag-scaffolds or cytokine cocktail (IL2/7/15). (**A**) Phenotypic distribution of KI
151 TCR/CAR T cells based on CCR7 and CD45RA expression, showing T_N ($CD45RA^+CCR7^+$), T_{CM} ($CD45RA^-$
152 $CCR7^+$), T_{EM}, and T_{EMRA} subsets. (**B**) CRISPR/Cas9 KI $CD8^+Tet^+$ T cells expressing $CD27^+CD28^+$ with
153 BV605-CD27 on y-axis and BUV737-CD28 on x-axis. (**C**) Graph showing the % $CD27^+CD28^+$ of $CD8^+Tet^+$

154 TCR/CAR KI T cells. (**D**) Graph showing the % of $CD8^+$ Tet^+ T cells expressing $PD1^+LAG3^+$ double positives.
155 **(E-F)** Graph showing the expression % of TCR T cells expressing CD107a and IFN-γ when re-stimulated with
156 target cells for 6 hrs. **(E)** Representative plot showing CRISPR/Cas9 KI $CD8^+Tet^+$ TCR T cells expressing
157 $CD107a^+$ IFN-γ^+ with PE-CD107a on y-axis and APC-IFN-γ on x-axis. **(F)** Graph showing the expression %
158 of T cells expressing IFN-γ, when re-stimulated with target cells for 6 hrs (left plot) normalised to the number
159 of NY-ESO-1-specific 1G4 TCR^+ T cells respectively (right plot). **(G)** Proliferative capacity of expanded
160 CRISPR/Cas9 KI CD19 CAR T cells, as measured by loss of Cell Trace Violet in a 6-day co-culture with
161 irradiated Jeko-1 target cells at an Effector: Target ratio of 1:5. **(H)** Representative histogram of cell trace
162 violet expression of CAR+ T cells on day 6 of restimulation. **(I)** Graph showing geometric MFI of the cell
163 trace violet on day 6. Data in (**B, F, H, I**) is from one experiment, and data in (**C**, **D**) is from 2-3 experiments
164 presented as mean ± SD and statistical significance determined by ratio-paired t-tests: *P < 0.05, **P < 0.01,
165 ***P < 0.001, ****P < 0.0001.

166 The expansion of engineered CAR T or TCR T cells yielded a product predominantly consisting of
167 terminally differentiated T_{EMRA} cells post-expansion in both cytokine and Ag-scaffold conditions
168 **(Figure 2A, Figures S2E-H)**. The expanded CAR T and TCR T cells had significantly higher
169 percentages of $CD27^+CD28^+$ cells and lower percentages of $CD27^-CD28^-$ cells, indicative of
170 enhanced self-renewal capacity **(Figures 2B-C, Figures S2I-J)**[22]. Notably, the TCR Ag-scaffold-
171 expanded T cells also had a significantly higher percentage of $PD1^+LAG3^+$ T cells compared to
172 IL2/7/15-expanded TCR T cells. This difference was not observed in CAR Ag-scaffold-expanded
173 CAR T cells **(Figure 2D, Figures S2K-I).**

174 To investigate the functional capacity of the expanded cell product, we incubated expanded 1G4 TCR
175 T cells with NY-ESO-1^+/HLA-A*02:01^+ A375 melanoma cells and evaluated production of IFN-γ,
176 TNF-α, and presentation of the CD107a marker of degranulation by intracellular cytokine staining.
177 A larger percentage of Ag-scaffold-expanded cells were positive for both IFN-γ, CD107a, and TNF-
178 α (**Figure 2F**, **Figures S3A-F**). This is likely a consequence of the larger proportion of the T cells
179 having the engineered TCR, as normalisation to the fraction of antigen-specific cells reduced this
180 difference (**Figures 2E-F, Figures S3G-I**). Together, these results indicated that the Ag-scaffold-
181 expanded T cells were at least on par with cytokine-expanded T cells in terms of producing IFN-γ
182 and TNF-α.

183 Given the high levels of CD28 and CD27 following Ag-scaffold expansion, we evaluated the
184 proliferative potential of Ag-scaffold-expanded CAR T cells and cytokine-expanded CAR T cells by
185 co-incubating CellTrace Violet-stained CAR T cells with $CD19^+$ Jeko-1 cells for 6 days followed by

evaluation of CellTrace Violet dilution (**Figure 2G**). We found that Ag-scaffold- and IL2/21-expanded CAR T cells proliferated the most following *in vitro* Jeko-1 challenge in accordance with the high CD28/CD27 expression (**Figures 2H-I, Figures S3M-N**). Together, this indicates that Ag-scaffold-expanded cells are effective at producing cytokines and possess a high proliferative capacity.

Given the phenotypical differences and increased proliferative capacity observed following Ag-scaffold expansion, we next evaluated the transcriptional differences between sorted Ag-scaffold- and cytokine-expanded NY-ESO-1-specific TCR T cells using single-cell RNA sequencing **(Figure 3A)** and bulk RNA sequencing **(Figures S4A-B)**. Unsupervised clustering of single-cell transcriptomes revealed distinct separation of CRISPR-engineered Ag-scaffold-expanded TCR T cells from their cytokine-expanded counterparts **(Figure 3B)** with similar findings for lentiviral-engineered TCR T cells **(Figure S5A)**, indicating broad transcriptional reprogramming driven by the expansion method. We observed the largest differences in gene expression when comparing Ag-scaffold-expanded cells and IL2/7/15 cells, with the negative regulators of TCR signalling, SOCS1 and CISH[23,24], being depleted in Ag-scaffold-expanded T cells **(Figures 3C-D, Figures S5B-C)**. We further observed an elevated expression of proliferation-associated genes, including PCNA, IL2RA, and MKI67, in Ag-scaffold-expanded T cells compared to both cytokine-expanded conditions, consistent with the high proliferative potential of Ag-scaffold-expanded T cells **(Figures 3C-E)**. In line with this observation, cell-cycle analysis demonstrated that approximately 50% of Ag-scaffold-expanded TCR T cells were in S or G2/M phase after 14 days of culture, confirming sustained cell-cycle activity **(Figure 3F, Figures S5D**).

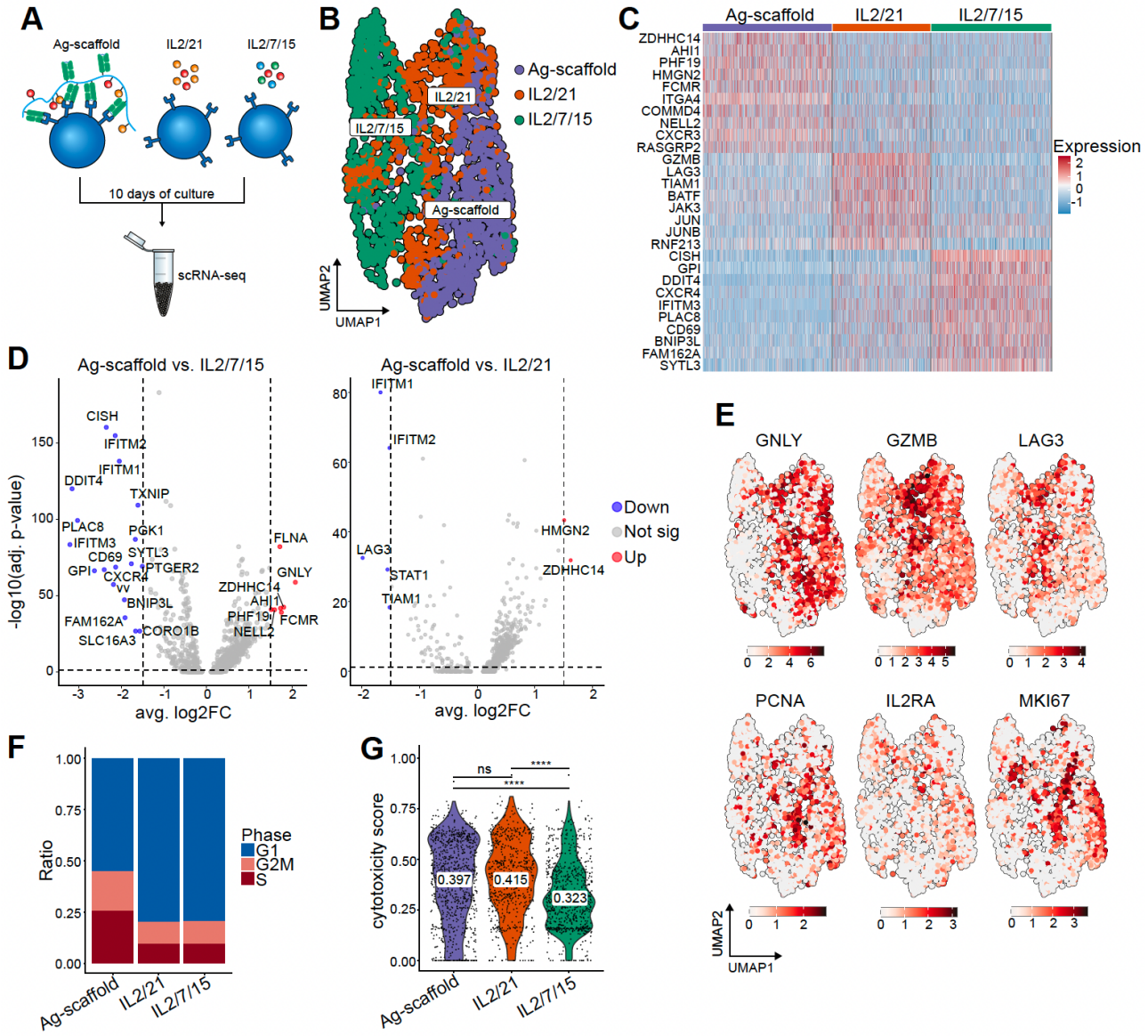

Figure 3. Single-cell RNA sequencing (scRNAseq) of CRISPR/Cas9-engineered T cells expanded with either Ag-scaffold, IL2/7, or IL2/7/15. (**A**) Diagram illustrating TCR T cells expanded with Ag-scaffold, IL2/21, or IL2/7/15 followed by 10x scRNAseq. (**B**) Uniform Manifold Approximation and Projection (UMAP) plot of all CRISPR/Cas9 engineered TCR T cells (total; 2,292 cells), with clusters colored and annotated according to cells expanded with either Ag-scaffold (total; 850 cells), IL2/21 (total; 647 cells), or IL2/7/15 (total; 795 cells). (**C**) Volcano plots showing differentially expressed genes for cells expanded with Ag-scaffold compared to IL2/7/15 (left) or IL2/21 (right). Genes significantly up- or down-regulated in the Ag-scaffold-expanded cluster are highlighted in red and blue, respectively. Dotted lines indicate thresholds on significance (log-fold-change =< 1.5 and p-value < 0.05 (-log10(0.05) = 1.3)). (**D**) UMAP plot of all CRISPR/Cas9 engineered TCR T cells showing the single cell mRNA expression levels of GNLY, GZMB, LAG3, PCNA, IL2RA, MKI67. (**E**) Expression of selected genes plotted on the UMAP from (D). (**F**) Barplot

218 showing the ratio of cells in each cell cycle phase (G1, S, G2/M) across the three expansion conditions. (**G**)
219 Violin plot illustrating cytotoxicity gene signature scores and means across the expansion conditions,
220 calculated from RNA expression of selected markers using UCell (GZMA, GZMB, GNLY, PRF1, ITGB1,
221 LAMP1). Statistics are calculated using Wilcoxon signed-rank test: ns = not significant, *P < 0.05, **P < 0.01,
222 ***P < 0.001, ****P < 0.0001.

223 Differential gene expression analysis further revealed upregulation of AHI1 and HMGN2, which are
224 implicated in cytokine-mediated proliferative signalling. In addition, Ag-scaffold-expanded T cells
225 displayed marked increases in cytotoxic effector transcripts such as GZMB, GNLY, and PRF1
226 compared to IL2/7/15-expanded T cells **(Figures 3C-E, Figures S5E-G)**. This pattern was also
227 observed in IL2/21-expanded cultures, suggesting that IL-2/21 signalling contributes to this cytotoxic
228 gene program **(Figure 3G)**. We observed higher levels of LAG3 in IL2/21-expanded T cells
229 compared to Ag-scaffold- and IL2/7/15-expanded T cells, suggesting a slightly more terminal
230 phenotype in these cells **(Figure 3E)**. Together, these findings indicate that Ag-scaffold expansion
231 drives a proliferative and cytotoxic effector phenotype distinct from that induced by soluble cytokine
232 expansion. Similar phenotypic patterns were observed following bulk RNA sequencing of Ag-
233 scaffold-expanded TCR T cells **(Figures S4A-B)**.

234 **Pooled tumour-shared antigen-specific CRISPR TCR T cells are effectively enriched by Ag-**
235 **scaffolds**

236 For TCR-based therapeutics, a challenge is the risk of tumour antigen-escape. To mitigate this, a pool
237 of TCRs could be used to target several cancer antigens. We therefore tested the ability of the Ag-
238 scaffold technology to stimulate and expand a pool of engineered TCR specificities. We engineered
239 T cells by CRISPR/Cas9 KI of 5 HLA-A*02:01-restricted tumour-shared antigen-specific TCRs from
240 the literature targeting NY-ESO-1/SLLMWITQC, MART-1/EAAGIGLTV[25],
241 gp100/IMDQVPFSV[26], SSX-2/KASEKIFYV[27], gp100/YLEPGPVTA[26]. For this, the T cells were
242 knocked in with a pool of all 5 homology-directed repair templates (HDRTs) and stimulated with a
243 pool of 5 different Ag-scaffolds carrying one specificity each (**Figure 4A**).

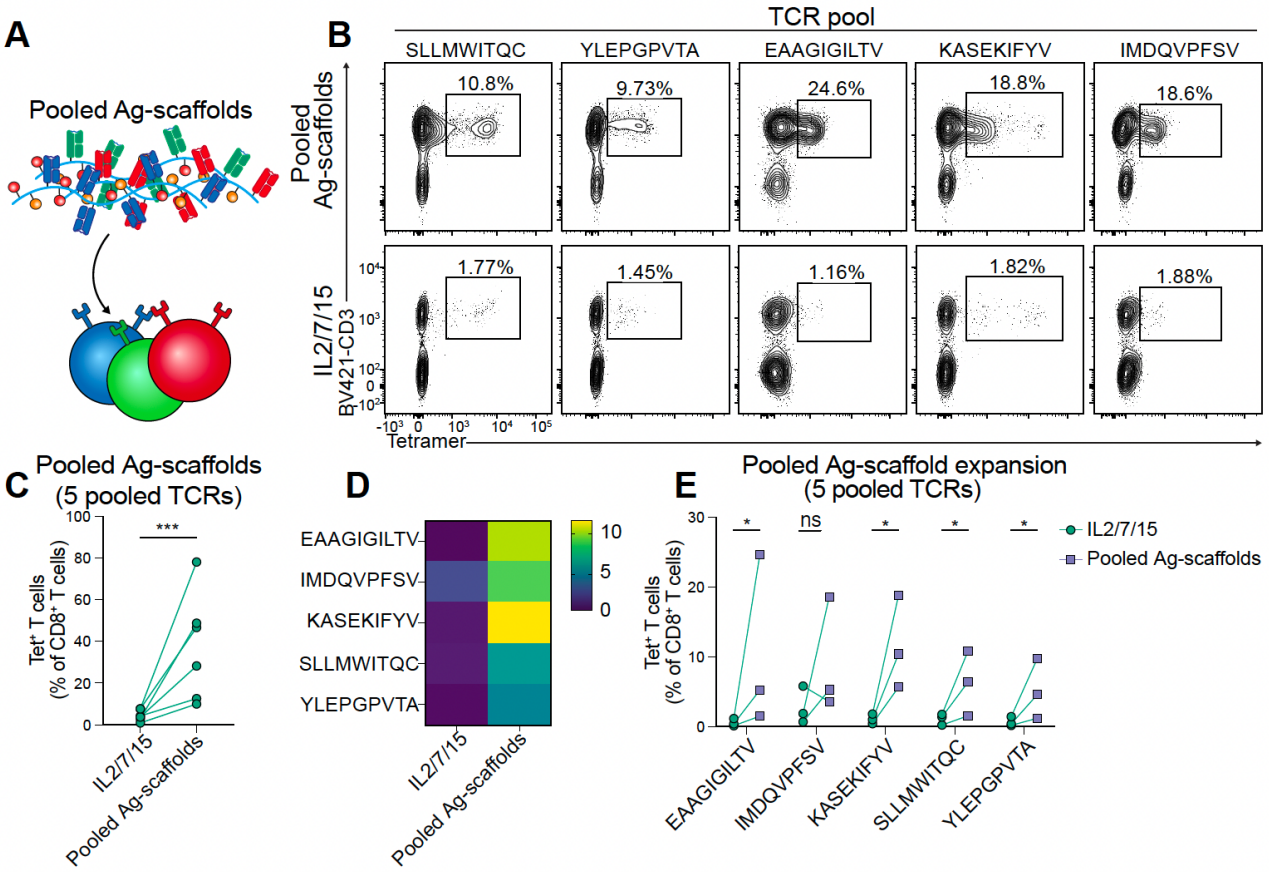

Figure 4. Pooled Ag-scaffold expansion of T cells engineered with a pool of TCRs. (**A**) Schematic depicting pooled Ag-scaffold expansion of a pool of T cells engineered to express 5 classical tumour shared antigen-specific HLA-A*02:01-restricted TCRs using CRISPR/Cas9 and representative flow plots showing percentages of Tet^{+} CD8^{+} T cells after 10 days of expansion using the pooled Ag-scaffolds or IL2/7/15. (**B**) Graph showing the total percentage of pooled tet^{+} CD8^{+} T cells after expansion (n=6 biological replicates from 2 experiments). (**C**) Heatmap showing the mean percentage of individual TCR Tet^{+} CD8^{+} T cells after expansion (n = 3). (**D**) Graph showing the % fold increase for each of the 5 KI TCRs in the culture following expansion with IL2/7/15 or Ag-scaffolds (n=3 biological replicates). Data in (**B**) is pooled from 2 experiments, and data in (**C, D**) is data from one experiment presented as dots for each data point in (**B, D**) and heatmap in (**C**). Statistical significance is evaluated by a ratio-paired T test in (**C**) and multiple ratio-paired t-tests with Holm-Šídák multiple comparison correction (**E**). P-values: *P < 0.05, **P < 0.01, ***P < 0.001, ****P < 0.0001.

Following 10 days of pooled expansion, we evaluated the expansion of the TCRs by staining using tetramers with separate fluorochromes per specificity. We found that the pooled expansions effectively expanded all 5 TCRs in the pool compared to the IL2/7/15 cytokine control from around 1-2 % to 10-25 % of CD8^{+} T cells **(Figure 4B).** When comparing the sum of all 5 specificities in

261 cytokine and Ag-scaffold conditions, the pooled expansions resulted in a significant enrichment of
262 the pool of antigen-specific T cells in the cultures **(Figure 4C).** It was clear that if the KI percentages
263 were high (cytokine control), Ag-scaffold expansion would achieve higher final percentages in the
264 cultures **(Figure 4C).** We observed specific expansion for all 5 TCRs in the pool **(Figures 4D-E)**
265 with significant expansion observed for 4/5 TCRs in the pool **(Figure 4E).** Collectively, this data
266 shows that the Ag-scaffold technology can be used to specifically expand a pool of TCRs following
267 CRISPR/Cas9 KI.

268 **Ag-scaffold-expanded engineered T cells are highly cytotoxic *in vitro* and *in vivo***

269 To evaluate cytotoxicity and functionality of Ag-scaffold-expanded TCR and CAR T cells,
270 CRISPR/Cas9 KI and lentiviral-modified TCR or CAR T cells were co-incubated with mCherry^{+}
271 target cells and imaged on the Incucyte platform **(Figure 5A)**. CAR T cells were subjected to 3
272 rechallenges with mCherry^{+} CD19^{+} Jeko-1 cells to evaluate cytotoxicity, whereas TCR T cells were
273 subjected to a single challenge with mCherry^{+} NY-ESO-1^{+}/HLA-A*02:01^{+} A375 melanoma cells,
274 and mCherry was imaged over 70 hours. First, we evaluated target cell killing following NY-ESO-1-
275 specific TCR T cells in coculture using a single challenge with mCherry^{+} A375 cells. We found that
276 Ag-scaffold-expanded NY-ESO-1-specific TCR T cells of both lentiviral and CRISPR/Cas9 origin
277 were more effective at killing the target cell line than cytokine-expanded cells **(Figure 5A-C)**.

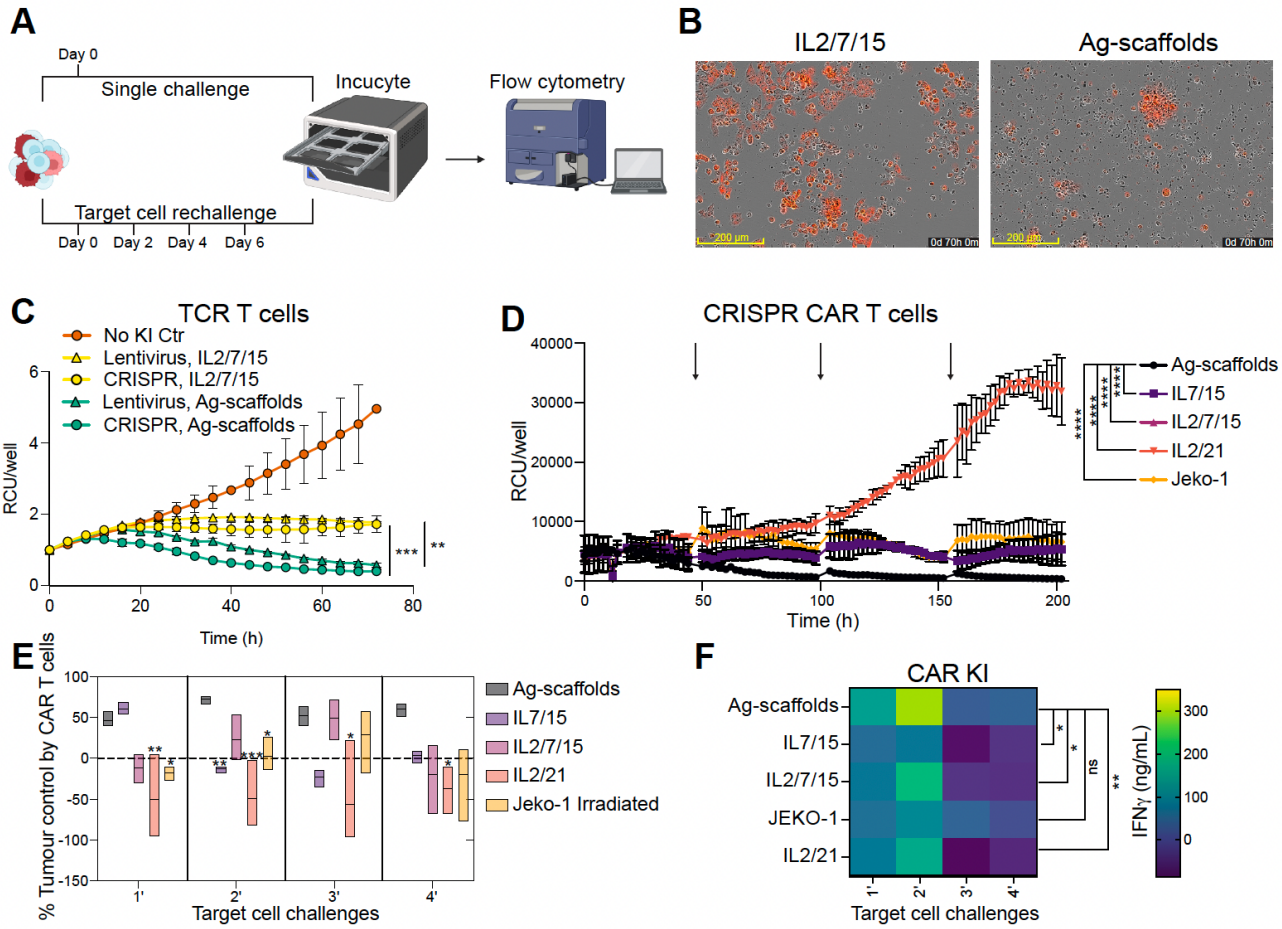

Figure 5. Antigen scaffold-mediated expansion yields CAR T cells that have high proliferative capacity, cytotoxicity, and cytokine production. (**A**) Schematic illustration of the Incucyte-based cytotoxicity re-challenge assay. (**B**) Representative images of mCherry^{+} A375 cancer cells after 70 hrs of coculture with cytokine-expanded (left) or Ag-scaffold-expanded (right) 1G4^{+} TCR T cells. Scale bar is 200 µm. (**C**) Cytotoxicity of CRISPR/Cas9 KI & Lentiviral 1G4^{+} TCR T cells in co-culture with mCherry^{+} A375 cells at an effector:target ratio of 1:1, tracked over 72 hours in the Incucyte, represented by relative confluence units (RCU) per well (representative of n=3 biological replicates). (**D**) Rechallenge cytotoxicity assay with CRISPR/Cas9 KI CAR T cells expanded with Ag-scaffolds, IL7/15, IL2/7/15, IL2/21, or Jeko-1 feeder cells mixed with mCherry^{+} Jeko-1 cells at a 1:1 effector:target ratio. CAR T cells were rechallenged with fresh Jeko-1 cells every 2 days (indicated by arrows), and cells were imaged for 200 hrs in the Incucyte, represented by relative confluence units (RCU) per well (representative of n=3 biological replicates). (**E**) Graph showing percentage tumour control by the CAR T cells over different target cell challenges calculated by %Tumour Control = (RCU at 48 hr – RCU at 0 hr)/(RCU at 0 hr)*100 (n=3 biological replicates from 1 experiment). (**F**) IFN-γ expression measured by ELISA in the supernatant (ng/mL) by CRISPR/Cas9 KI and lentiviral CAR T cells after every 48 hrs of target cell challenge as described in (**D**, **E**). (**C-F**) Statistical significance was determined using ordinary one-way ANOVA with Šídák's multiple comparisons. In (**C**) the multiple

295 comparison is comparing cytokine with Ag-scaffold for lentiviral and CRISPR/Cas9 conditions. In (**D**), the
296 multiple comparisons compare Ag-scaffold to other groups. In (**E**) Ag-scaffold conditions were compared to
297 all other groups within each timepoint by multiple comparisons (indicated with asterisks above the compared
298 groups when P<0.05). In (**F**), the multiple comparisons compare the groups in the last rechallenge. P-values:
299 *P < 0.05, **P < 0.01, ***P < 0.001, ****P < 0.0001.

300 Secondly, we evaluated CD19 CAR T cell cytotoxicity in a rechallenge assay with Jeko-1 cells as
301 target cells, with rechallenges every 48 hours to simulate *in vivo* challenges. We found that Ag-
302 scaffold-expanded CAR T along with irradiated Jeko-1- and IL7/15-expanded cells exhibited superior
303 tumour control and cytotoxicity over the first two rounds of target cell rechallenges. However, Ag-
304 scaffold-expanded CAR T exhibited significantly higher tumour control against $CD19^{hi}$ Jeko-1 cells
305 across rechallenges **(Figures 5A, D, E,** and **Figures S6A, B, C).** Normalised tumour control
306 calculations revealed significantly higher tumour suppression by Ag-scaffold-expanded CAR T cells
307 compared to those expanded with conventional cytokine cocktails.

308 Supernatants collected every 48 hours before each rechallenge revealed that Ag-scaffold-expanded
309 CAR T cells secreted significantly higher levels of IFN-γ throughout all rechallenges than cytokine-
310 expanded cells **(Figure 5F, Figure S6B).** Further, following rechallenges we evaluated the T cells by
311 flow cytometry and observed that the Ag-scaffold-expanded CAR T cells had higher proportions of
312 T_{CM} cells and lower percentages of terminally differentiated CAR T cells **(Figures 5C-F, Figures**
313 **S6D-G)**

314 Finally, we tested the *in vivo* tumour-killing capacity of the CRISPR-engineered CD19 CAR T cells
315 expanded with Ag-scaffolds or IL2/7/15 in NSG mice pre-inoculated with Jeko-1 lymphoma cells
316 engineered to express luciferase (luc-$mCherry^{+}$), allowing for tracking of tumour growth by
317 bioluminescence (BLI). We evaluated a low dose of 0.25 and $0.5x10^6$ CAR T cells administered
318 intravenously 7 days post inoculation to investigate the functional difference between the cytokine-
319 expanded and Ag-scaffold-expanded CAR T cells. The mice were scanned using IVIS to monitor the
320 change in BLI every 7 days after ACT. We found that treatment with CAR-T cells expanded with
321 Ag-scaffolds resulted in complete tumour control in both the $0.25x10^6$ and $0.5x10^6$ CAR T cell groups
322 until day 33 post treatment **(Figures 6A-B)**. The IL2/7/15 cytokine-expanded CAR T cells showed
323 no significant tumour control with the lowest dose of $0.25x10^6$ CAR T cells, when compared to the
324 no KI T cells, leading to the euthanisation of 4/5 mice by day 21 **(Figure 6B)**. The higher dose of
325 $0.5x10^6$ cytokine-expanded CAR T cells slowed tumour growth until day 21 after which all mice had
326 a significantly higher tumour burden when compared to the mice treated with Ag-scaffold-expanded

CAR T cells **(Figure 6B)**. The mice were euthanised on day 33 and spleen and bone marrow were collected for the detection of CAR T cells by flow cytometry. We found that Ag-scaffold-expanded CAR T cells were present at significantly higher percentages and numbers in the spleen, but not in the bone marrow, compared to the cytokine-expanded T cells **(Figures 6C-D)**.

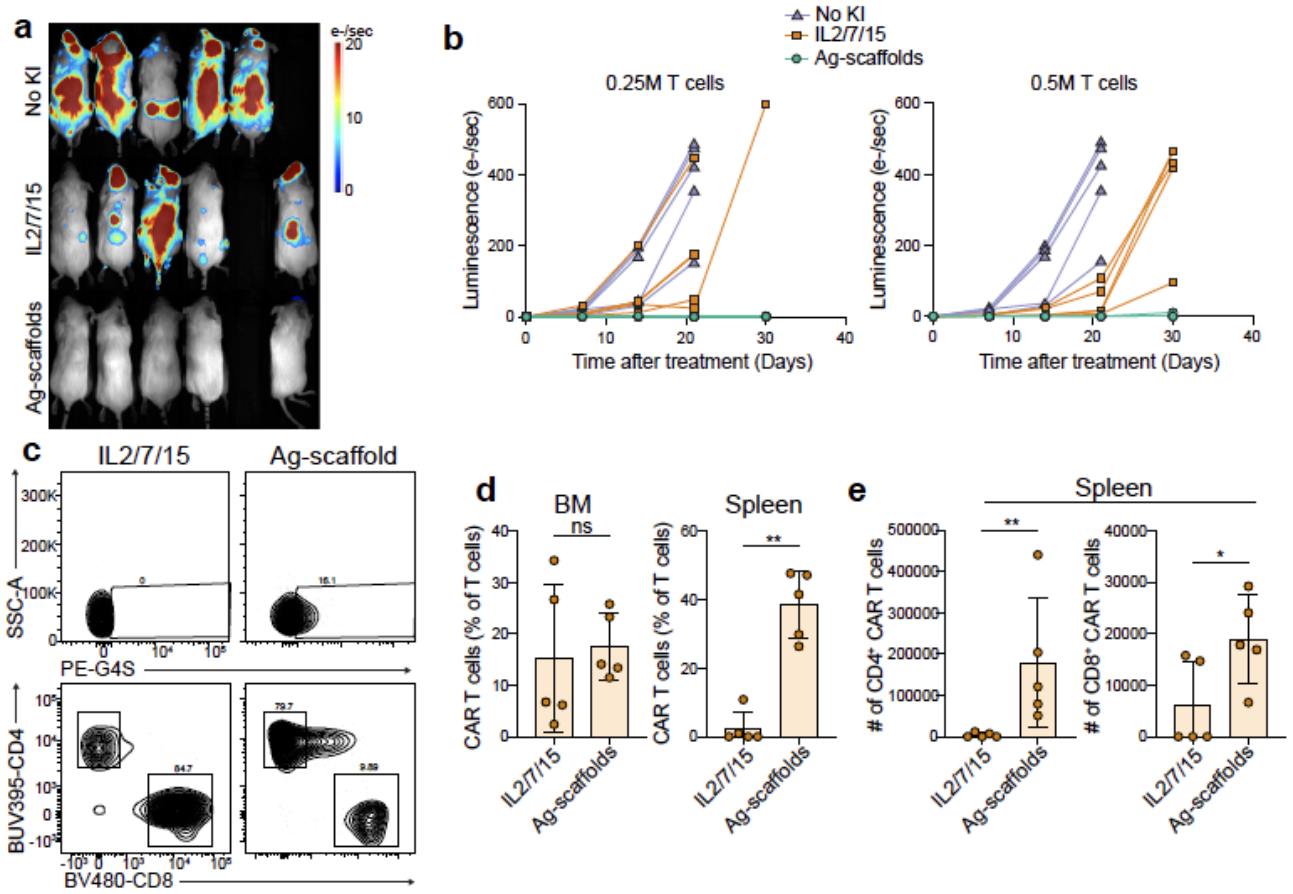

Figure 6. Antigen-scaffold-expanded CAR T cells are effective killers *in vivo* in NXG xenograft models. (**A**) BLI luminescence quantification of luciferase signal day 21 after intravenous inoculation of Luciferase-transduced JEKO-1 cell in immunodeficient NXG mice (n=5 mice per group) and injection of $0.5x10^6$ CAR T cells expanded with IL2/7/15 or Ag-scaffolds on day 7. Cell numbers were adjusted for the actual number of CAR-expressing T cells. **(B)** Quantification of cancer cell growth from luminescence signal (e-/sec) over time following injection of $0.25x10^6$ or $0.5x10^6$ CAR T cells 7 days after jeko-1 injection (n=5 mice per group). Mice were terminated when a predefined humane endpoint was reached. **(C-E)** On day 30, spleens and bone marrow (BM) from the IL2/7/15 and Ag-scaffold-expanded 0.5 $x10^6$ CAR T cell groups were analysed by flow cytometry, and CAR T cell percentages. (**C**) Representative flow plots showing $CD3^+$ CAR T cell population (top) and $CD3^+CD4^+$ & $CD3^+CD8^+$ T cells (bottom), and number of CAR T cells (**D**) were quantified. Statistical significance in (**C, D**) determined by ratio-paired t-test: *P < 0.05, **P < 0.01, ***P < 0.001, ****P < 0.0001.

344 **Discussion**

345 The substantial clinical efficacy of CAR T-cell therapy in treating haematological malignancies has
346 brought significant attention to engineered T-cell therapies. However, the clinical production of these
347 therapies faces several bottlenecks often resulting in final products with T cells of poor persistence
348 and impaired function leading to suboptimal efficacy[11]. One major contributing factor to the
349 compromised quality of T-cell products is the intense initial activation induced by anti-CD3 and anti-
350 CD28 antibodies, followed by stimulation from recombinant cytokines. These cytokines are typically
351 added in high concentrations to achieve clinically relevant numbers of specific T cells, often leading
352 to T-cell exhaustion[28].

353 The renewal and persistence of T-cell products are closely tied to the type and strength of co-
354 stimulation and activation. An alternative to activation through CD3/CD28 cross-linking involves the
355 use of irradiated target cells expressing the CAR antigen as feeder cells, which supports the expansion
356 of antigen-specific T cells[29]. However, CAR products generated by this method show no significant
357 functional improvement compared to those produced using conventional protocols and the co-
358 stimulatory signals provided to the T cells can be difficult to tailor to a particular phenotype.
359 Furthermore, the potential risk of re-infusing viable target cells into patients complicates the cGMP
360 production of these products[30].

361 Recently, a wave of innovation in bio-compatible and degradable materials for micro- and nanoscale
362 aAPCs designed to expand antigen-specific T cells has emerged[18,31]. These aAPCs offer the
363 advantage of creating customisable, off-the-shelf products targeting multiple specificities of TCRs
364 and CARs. Additionally, their small size provides a spatial advantage by enabling paracrine delivery
365 of cytokines and co-stimulation directly to antigen-specific cells upon engagement.

366 We recently developed a novel dextran scaffold-based technology and described how it is an effective
367 tool for expanding endogenous viral and tumour antigen-specific $CD8^+$ T cells[20]. Our previous
368 research demonstrated the modularity of the streptavidin backbone, which facilitates the attachment
369 of pMHC, and costimulatory cytokines such as IL2 and IL21 used in this study[21]. Building on this
370 foundation, we hypothesised that this technology could be extended to enhance CAR and TCR T cell
371 products. Especially the relatively low KI efficacy of CRISPR/Cas9-engineered T cells highlights the
372 need to enrich engineered antigen-specific T cells without compromising their phenotype and
373 functionality[6].

374 Our results show that the average KI percentage is >15% in both TCR (~15%) and CAR (~6%) using
375 Cas9 RNPs with double-stranded DNA HDR templates. The NY-ESO-1/HLA-A*02:01 pMHC Ag-
376 scaffold supported expansion of NY-ESO-1 CRISPR/Cas9 TCR T cells, leading to a T-cell product
377 with >90% TCR T cells. Similarly, the CD19 CRISPR/Cas9 CAR T cells expanded with CD19 CAR
378 Ag-scaffold led to a ~400-fold specific expansion of CAR T cells, reaching >60% CAR T cells on
379 day 10 of expansion. Both yield a T-cell product that is significantly enriched compared to their
380 cytokine-cocktail- and irradiated target cell-expanded counterparts. The strategy is likely also
381 applicable to other receptor modalities, such as T cells engineered to present *de novo*-designed pMHC
382 minibinder as antigen receptors[32–34].

383 Ag-scaffold-expanded lentiviral and CRISPR/Cas9 TCR T cells exhibited robust proliferation while
384 maintaining an efficacious early effector phenotype. These cells showed high expression of CD27
385 and CD28, markers associated with enhanced proliferative capacity and effector function, in contrast
386 to cells expanded with IL2/7/15. The $CD27^{+}CD28^{+}$ phenotype has been correlated with improved
387 disease prognosis in cancer immunotherapy[7,10,35]. Consequently, the Ag-scaffold-expanded 1G4 TCR
388 T cells showed superior functionality in *in vitro* cytotoxicity assays in comparison to the IL2/7/15-
389 expanded TCR T cells.

390 Ag-scaffold-expanded CAR T cells also showed remarkable functionality. Upon antigen re-
391 stimulation, Ag-scaffold-expanded CAR T cells exhibited high proliferative capacity. These cells
392 exhibited sustained tumour cell killing over four rounds of rechallenge, whereas CAR T cells
393 expanded using conventional cytokines lost their cytotoxic capacity after two rounds of rechallenge.
394 Moreover, Ag-scaffold-expanded CAR T cells consistently produced higher levels of IFN-γ during
395 rechallenge assays.

396 Upon re-encountering antigen, previously primed T cells integrate signals from the TCR, co-
397 stimulatory receptors, and cytokines to determine their fate: balanced stimulation drives further
398 activation and differentiation into memory subsets (such as T_{CM} or T_{SCM}), whereas excessive or
399 prolonged signalling triggers activation-induced cell death (AICD)[36]. Serial antigen stimulation leads
400 to T-cell exhaustion with high expression of markers of exhaustion[36,37]. We evaluated the efficacy of
401 the Ag-scaffold-expanded CAR T cells in a relevant B-cell lymphoma xenograft mouse model. Even
402 when the number of antigen-specific cells was normalised, the Ag-scaffold-expanded cells still
403 outperformed the cytokine-expanded cells in clearing cancer cells. This strongly indicates that the

404 Ag-scaffold-expansion drives a favourable phenotype, in addition to enriching the antigen-specific
405 proportion of the cell product.

406 A significant limitation of TCR and CAR T-cell therapies for solid tumours is the heterogeneity of
407 tumour antigen expression. Addressing this challenge often requires engineering T-cell pools with
408 multiple specificities, but the bottleneck of low KI efficacy remains a barrier to producing clinically
409 relevant products[4]. We demonstrated that scaffold technology could effectively enrich T cells
410 engineered with different specificities, paving the way for customisable and efficient production of
411 multi-specific T-cell products.

412 In conclusion, antigen- and cytokine-mediated activation and expansion using scaffold technology
413 yielded highly enriched CAR and TCR T-cell products with superior potency *in vitro* and *in vivo*
414 compared to conventional methods. These Ag-scaffold-expanded T cells demonstrated enhanced
415 proliferation, sustained cytotoxicity, and improved cytokine production; *in vivo* superiority was
416 established in a $CD19^+$ lymphoma xenograft, and generalisation to TCR-engineered products and
417 additional tumour models will be determined in future studies.

418 Limitations of the study

419 While our study demonstrates that Ag-scaffolds can drive the preferential expansion of functional,
420 genetically engineered T cells, several limitations warrant consideration. First, the *in vivo* efficacy of
421 Ag-scaffold-expanded T cells was demonstrated exclusively using the CD19 CAR T cell model in a
422 B-cell lymphoma xenograft. Although we established the *in vitro* cytotoxicity and phenotypic
423 superiority of Ag-scaffold-expanded TCR T cells, the translational potential of the TCR-engineered
424 products remains to be validated in relevant solid tumour animal models. Future studies will also have
425 to evaluate safety of Ag-scaffold-expanded cells. Second, the starting material for all experiments
426 consisted of peripheral blood mononuclear cells (PBMCs) obtained from healthy donors. T cells
427 derived from heavily pre-treated cancer patients often exhibit compromised fitness and distinct
428 baseline exhaustion profiles compared to healthy donors. Consequently, the expansion efficiency and
429 functional rejuvenation observed here require validation using patient-derived material to fully
430 ascertain clinical applicability.

431 Resource availability

432 Lead contact

Further information and requests for resources and reagents should be directed to the lead contact Sine Reker Hadrup (sirha@dtu.dk).

Materials availability

All reagents/materials generated in this study will be made available upon request. The request may require a completed Material Transfer Agreement.

Data and code availability

Single-cell RNA-seq data have been deposited at the Gene Expression Omnibus (GEO) and are publicly available as of the date of publication. Accession numbers are listed in the Key Resources Table. All code used is publicly available as described in STAR Methods. Any additional information required to reanalyse the data reported in this paper is available from the lead contact upon request.

Acknowledgements

We thank Sébastien Sebbaha from the Flow Cytometry and Imaging Core (FLIC) at DTU Health Tech, for flow cytometry experiments. We thank technicians Thi Minh Lien Nguyen and Panchale Olsen for assistance with cell cultures and ELISA.

The project was funded partly by a postdoctoral Lundbeck Foundation fellowship [R347-518 2020-2174] and the Novo Nordisk Foundation (Challenge program, Nano-Immune-Cell-Engineering, NICE) [NNF21OC0066562], European Union's Horizon 2020 research and innovation program Marie Curie international training network, T-OP [955575].

Author Contributions

Shared authors have contributed equally and are listed alphabetically by last name, and they are free to change the order on their CVs. S.R.H., K.H.J., K.R., and M.O. conceived the project and provided funding. S.R.H. and M.O. supervised the work. K.R., K.H.J., S.R.H., and M.O. wrote and reviewed the manuscript. K.H.J., K.R., C.R.P., A.K.G., L.F.V., H.R.H., S.T., L.S.G., E.D., A.H.S., L.P.F., M.B., and M.S.F. performed experimentation and analysis for the manuscript. All authors approved of the manuscript.

Declaration of interest

S.R.H. is inventor on patents (EP2017/083862 and EP3810188A1) on the Ag-scaffold technology. The remaining authors declare no competing interests.

462 # Materials and Methods

463 **Key Resources table:**

Resources	Source	Identifier
Antibodies		
Anti-human CD3 (Clone OKT-3)	BioXcell	Cat# BE0001-2
Anti-human CD28 (Clone 9.3)	BioXcell	Cat# BE0248
Anti-human CD3 (Clone UCHT1)	BioLegend	Cat# 300465
Anti-human CD28 (Clone CD28.2)	BioLegend	Cat# 302943
BB700-anti-human CD25 (IL-2R) (Clone M-A251)	BD Biosciences	Cat# 566447
BV786-anti-human CD69 (Clone FN50)	BD Biosciences	Cat# 563834
PE-anti-human CD69 (Clone FN50)	BioLegend	Cat# 310906
BV421-anti-human CD3 (Clone SP34-1)	BD Biosciences	Cat# 562877
BV711-anti-human CD45RA (Clone HI100)	BD Biosciences	Cat# 563733
APC-anti-human CD197 (CCR7) (Clone 2-L1-A)	BD Biosciences	Cat# 566762
PE/Cy7-anti-human TIM-3 (Clone F38-2E2)	BioLegend	Cat# 345014
BUV737-anti-human CD279 (PD-1) (Clone EH12.1)	BD Biosciences	Cat# 612791 / 565299
BV650-anti-human CD223 (LAG-3) (Clone 11C3C65)	BD Biosciences	Cat# 369316
PE-Cy7-anti-human CD57 (Clone QA17A04)	BioLegend	Cat# 393310 / B323195
BV786-anti-human CD39 (Clone TU66)	BD Biosciences	Cat# 742523
BV605-anti-human TIGIT (Clone 741182)	BD Biosciences	Cat# 747841
BV480-anti-human CD4 (Clone L200)	BD Biosciences	Cat# 566148
PerCP-anti-human CD8 (Clone SK1)	BD Biosciences	Cat# 347314
BV480-anti-human CD8 (Clone RPA-T8)	BD Biosciences	Cat# 566121
BUV737-anti-human CD28 (Clone CD28.2)	BD Biosciences	Cat# 612815
BV605-anti-human CD27 (Clone O323)	BioLegend	Cat# 302830
PE-anti-human CD137 (Clone 4B4-1)	BD Biosciences	Cat# 555956
PE/Cy7-Streptavidin	BD Biosciences	Cat# 557598
BV711-anti-CD19 (Clone SJ25C1)	BD Biosciences	Cat# 563036

PE-Cy7-anti-CD4 (Clone RPA-T4)	BD Biosciences	Cat# 560649
Purified Mouse Anti-Human IFN-γ	BD Biosciences	Cat# 551221
Biotin Mouse Anti-Human IFN-γ	BD Biosciences	Cat# 554550
TotalSeq-C Human Universal Cocktail V1.0	BioLegend	Cat# 399905
Human TruStain FcX™ Blocking Reagent	BioLegend	Cat# 422302
Bacterial and Virus Strains		
NEB Stable Competent E. coli	New England Biolabs	Cat# C3040I
Biological Samples		
Human PBMCs	Rigshospitalet, Copenhagen	N/A
Chemicals, Peptides, and Recombinant Proteins		
Biotinylated Human CD19 (20-291) Protein	Acro Biosystems	Cat# 20-291(His,Avitag)
Recombinant Human IL-2 (Avitag)	Acro Biosystems	Cat# IL-2H82F3
Recombinant Human IL-21 (Avitag)	Acro Biosystems	Cat# IL-21-H82F7
Recombinant Human IL-2	Peprotech	Cat# 200-02-250UG
Recombinant Human IL-7	Peprotech	Cat# 200-07-100UG
Recombinant Human IL-15	Peprotech	Cat# 200-15-50UG
Cas9 Nuclease V3	IDT	Cat# 10000735
TRAC crRNA	IDT	N/A
tracrRNA	IDT	N/A
ssODN (Electroporation Enhancer)	IDT	N/A
M3814 (DNA-PK inhibitor)	Selleckchem	Cat# S8586
Dasatinib	LC Laboratories	Cat# D3307
LIVE/DEAD™ Fixable Near-IR Dead Cell Stain	Invitrogen	Cat# L34976
CellTrace™ Violet	Invitrogen	Cat# C34557
TMB Substrate	Kem-en-Tec	Cat# 4380A
Streptavidin-POD Conjugate	Merck	Cat# 11089153001
D-Biotin	Sigma-Aldrich	Cat# B4501
Peptides (Custom synthesized)	SB Peptides	N/A
Critical Commercial Assays		
MojoSort™ Human CD3 T Cell Isolation Kit	BioLegend	Cat# 480131
NEBuilder HiFi DNA Assembly Master Mix	New England Biolabs	Cat# E2621S
P3 Primary Cell 4D-Nucleofector™ X Kit	Lonza	Cat# V4XP-3032
Chromium Next GEM Single Cell 5' Kit v2	10x Genomics	Cat# 1000263
Deposited Data		

Single-cell RNA-seq data	This paper	GEO: [ACCESSION NUMBER NOT AVAILABLE YET]
Experimental Models: Cell Lines		
Jeko-1	ATCC	CRL-3006
A375	ATCC	CRL-1619
HEK-293T	ATCC	CRL-3216
SUP-T1	ATCC	CRL-1942
Experimental Models: Organisms/Strains		
NXG Mouse	Janvier Labs	NOD-Prkdcscid-IL2rgTm1/Rj
Oligonucleotides		
Primers for TCR/CAR HDRT assembly	IDT	Table S1
Recombinant DNA		
pRSV.REV	Addgene	RRID: Addgene_12253
pMDLg/p.RRE	Addgene	RRID: Addgene_12251
pMD2.G	Addgene	RRID: Addgene_12259
TCR and CAR HDRT	Twist Bioscience	Table S1
Software and Algorithms		
FlowJo v10.10.0	BD Biosciences	https://www.flowjo.com
GraphPad Prism v10.5.0	GraphPad Software	https://www.graphpad.com
Cell Ranger 7.0.0	10x Genomics	https://support.10xgenomics.com
Seurat v5.3.0	Satija Lab	https://satijalab.org/seurat
SCpubr v3.0.0	Enblacar	https://github.com/Enblacar/SCpubr
UCell v2.12.0	Carmona et al.	https://github.com/carmonalab/UCell
Kallisto Quant	Pachter Lab	https://pachterlab.github.io/kallisto
DESeq2	Love et al.	https://bioconductor.org/packages/DESeq2
Trim Galore	Babraham Bioinformatics	https://www.bioinformatics.babraham.ac.uk
Other		
AccuDrop™ Beads	BD Biosciences	Cat# 345249
16-well Nucleocuvette™ Strip	Lonza	Cat# V4XP-3032
SepMate™ Tubes	StemCell Technologies	Cat# 86460

Experimental model and study participant details

PBMCs

PBMCs were sourced from healthy donors from Rigshospitalet, Copenhagen, approved by the Danish ethics committee. PBMCs were isolated from whole blood by density centrifugation using SepMate tubes (StemCell) and frozen in liquid nitrogen in FBS and 10 % DMSO.

T cell cultures

Cryopreserved PBMCs were thawed and washed in RPMI-1640 GlutaMAX™ + 10 % FBS (R10 medium), and T cells were isolated by negative selection using MojoSort™ Human CD3 T Cell Isolation Kit (Biolegend) according to the manufacturer's instructions. Cells were counted and

474 activated on 5 µg/mL plate-bound anti-CD3 (clone: UCHT1, Biolegend) with 2 µg/mL soluble anti-
475 CD28 (clone: 28.2, Biolegend) in X-vivo-15 (Lonza, BE02-060Q) + 5 % human serum (Sigma
476 Aldrich Heat Inactivated H3667), supplemented with 200 IU/mL recombinant human IL2
477 (Peprotech), 5 ng/ml IL7 (Peprotech), and 5 ng/ml IL15 (Peprotech).

478 **Cell lines and culture**

479 The human cell lines Jeko-1 (B cell lymphoma) and A375 (melanoma) were obtained from American
480 Type Culture Collection (ATCC) and cultured in RPMI supplemented with 10% fetal bovine serum
481 and 1% penicillin-streptomycin.

482 For cytotoxicity assay and *in vivo* tumour models, these cell lines were transduced with mCherry-Luc
483 lentiviral vector (**Table S1**) and were sorted on a FACSmelody (BD Biosciences) to establish new
484 cultures.

485 **In vivo NXG tumour xenograft models**

486 The Danish National Animal Experiment Inspectorate and the institutional ethics board at the
487 Technical University of Denmark approved all procedures (License#2020-15-0201-00748). For the
488 efficacy study, 7–10-week-old female immunodeficient NXG mice (NOD-Prkdcscid-IL2rgTm1/Rj;
489 Janvier Labs) were intravenously injected with 1×10^6 luciferase-expressing Jeko-1 cells. After a 7-
490 day tumour engraftment period, mice were randomised and injected intravenously with either the Ag-
491 scaffold- or IL2/7/15-expanded CD19 CAR T cells in 200 µL PBS. Effector:target ratios were
492 adjusted to the CAR-positive fraction, i.e., the number of cells shown is the number of CAR^+ T cells.
493 Tumour burden was monitored weekly by bioluminescence imaging (Optical Imaging unit, MILabs).
494 For imaging, mice were injected intraperitoneally (i.p.) with D-Luciferin (3 mg/mouse) and imaged
495 20 minutes later. Luminescence was then quantified using fixed-size regions of interest. Body weight
496 and general health were monitored throughout the study. At termination, single-cell suspensions of
497 spleen and bone marrow were prepared for flow cytometry. Spleens were processed through a 70 µm
498 filter, followed by red blood cell lysis. Cells were then stained with a viability dye (Near-IR) and
499 antibodies for CD3, CD4, CD8, CD45RA, CCR7, and a CD19 CAR tetramer before analysis on an
500 LSRFortessa™.

501

502 ## Method details

503 **Preparation of dsDNA homology-directed repair template**

504 The HDRTs used for KI of the NY-ESO-1-specific 1G4 TCR were designed as follows: 5' HA (300
505 bp)-T2A-TCRb-furin cleavage site-SGSG linker-P2A-TCRa variable chain-3' HA (300 bp)[4,38],
506 whereas HDRTs used for KI of CARs were designed as follows: 5' HA (300 bp)-T2A-scFv-CD8
507 hinge/transmembrane domain-41BB/CD3z signalling domain-bGH polyA-3' HA (300 bp) (Table
508 S1). For the four other TCRs, a 500 bp 3' and 5' HA was used. TCR constructs were ordered as clonal
509 genes (Twist Bioscience), CAR constructs were assembled by HiFi assembly (NEB, E2621S).
510 Briefly, we performed PCR of the backbone from the TCR HDR plasmid containing the TRAC HDR
511 homology arms (primers: TCR_HDR_HiFi_fwd, TCR_HDR_HiFi_rev), the CD19 CAR gene from
512 the lenti_CD19_CAR plasmid (primers: CD19 plasmid_fwd, CD19 plasmid_rev), and a bGH polyA
513 tail (primers: pA AAVS1 plasmid_fwd, pA AAVS1 plasmid_rev) and purified using a PCR clean-
514 up kit (Qiagen, #28104). The PCR fragments were mixed in a HiFi reaction according to the
515 manufacturer's instructions, followed by transformation in NEB Stable bacteria (NEB, #C3040I).
516 Assembled plasmids were sequence verified. The HDRTs were amplified from the plasmids using
517 TRAC_HDRT_1.Fwd and TRAC_HDRT_1.Rev primers (**Table S1**) with Herculase Fusion II
518 polymerase with the following PCR program: 1 cycle of 95°C, 5 min. 34 cycles of 95°C, 20 sec;
519 63°C, 20 sec; 72°C, 1.5 min. 1 cycle of 72°C, 3 min. TRAC_HDRT_2.Fwd and TRAC_HDRT_2.Rev
520 were used for 500 bp HAs. Products were purified using 1:1 volume homemade Ampure XP beads[39].
521 Concentration of dsDNA HDRT was measured by Nanodrop, and products were validated by gel
522 electrophoresis.

523 **Non-viral CRISPR/Cas9-mediated KI**

524 Our non-viral CRISPR/Cas9-mediated KI protocol was adapted from previous publications[4,40].
525 Briefly, gRNAs were prepared by mixing equimolar ratios of 200 µM TRAC_crRNA and tracrRNA
526 (IDT) resuspended in duplex buffer, and incubated at 95°C for 5 min or 37°C for 30 min and slowly
527 cooled to RT. To prepare Cas9 RNPs, 3 µL of PBS, 1.2 µL of 100 µM gRNA, and 1 µL of Cas9
528 (62µM Cas9 nuclease V, IDT) were mixed and incubated at RT for 15 min. 0.5 µL of scrambled
529 Single-stranded oligodeoxynucleotides was added as electroporation enhancer (ssODN, 200 µM,
530 IDT). 1 µg of double-stranded HDRT was added 1 min before mixing with T cells for nucleofection.

531 $1x10^6$ T cells per nucleofection cuvette were counted and spun down at 100xG for 10 min and
532 resuspended in 20 µL RT P3 buffer (Lonza). RNP/HDRT mix was added, and cells were transferred

533 to a 16-well nucleofection cuvette (Lonza) and nucleofected with pulse-code EH115 on a 4D-
534 nucleofector. 80 µL of incubator equilibrated X-vivo-15 without serum or cytokines was added and
535 cells were incubated for 30 min. Cells were transferred to a 48 well plate at $2x10^6$ cells/well in X-
536 vivo-15 + 5 % HS + 200 IU/mL rhIL2, 5 ng/mL IL7, 5 ng/mL IL15, and DNA-PK inhibitor 1 µM of
537 M3814 (S8586, Selleckchem). M3814 inhibitor was removed the next day. KI was evaluated 2-3 days
538 after nucleofection.

539 **Lentiviral transduction of T cells**

540 The CAR/TCR was inserted into a third-generation lentiviral vector under the control of a human
541 EF1α promoter. All plasmids were synthesised by GenScript, USA. Lentiviral particles were
542 generated in HEK-293T cells by transfecting them with three separate packaging plasmids:
543 pRSV.REV(Addgene plasmid #12253), pMDLg/p.RRE (Addgene plasmid #12251), and pMD2.G
544 (Addgene plasmid #12259) were a gift from Didier Trono[41], along with a transfer plasmid containing
545 the DNA construct of interest. The titer of the produced lentivirus particles was assessed through a
546 titration experiment by infecting SUP-T1 cells and subsequently analysing GFP or surface expression
547 of the receptor via tetramer staining via flow cytometry.

548 The T cells were activated $2x10^6$ cells/mL for 48 hrs at 37°C and 5% CO_2 in x-vivo-15 media (Lonza)
549 supplemented with 5% human serum containing recombinant IL2 (200IU/mL), IL7 (5ng/mL), IL15
550 (5ng/ml) (Preprotech, USA) and anti-CD3 and CD-28 (5ng/ml). After the activation period, the T
551 cells were washed and resuspended in x-vivo-15 media (Lonza) supplemented with 5% human serum
552 and transduced with the required amount of lentivirus at a multiplicity of infection (MOI) of 1 and
553 expanded for another 10 days.

554 **Preparation of peptide MHC**

555 pMHC monomers and pMHC tetramers were prepared as previously described[42,43]. Briefly, the
556 peptides were synthesised and acquired from SB peptides and resuspended in DMSO at 10 mM, and
557 in-house produced avitagged-HLA-A*02:01^{Y84C} was used for peptide loading (final conc.: 100µg/ml
558 HLA; 200 µM peptide) at RT for 30 min prior to tetramerising with PE- or APC-labelled streptavidin
559 for 30 min on ice and blocking with D-biotin 20 min on ice prior to freezing in 0.5% BSA and 5%
560 glycerol at -20°C.

561 **Antigen scaffold generation**

562 Ag-scaffolds were assembled, using a streptavidin-conjugated dextran backbone (500 kDa) (Fina
563 Biosolutions) mixed with biotinylated peptide MHC class I complex or CAR antigen (CD19 Avitag,

564 Acro Biosystems), IL-2 Avitag (Acro Biosystems #IL-2H82F3), and IL-21 Avitag (Acro Biosystems
565 #IL-21-H82F7), followed by incubation at 4°C for 30 min. Ag-scaffolds were incubated with D-
566 Biotin at 4°C for 20 min to block potential free streptavidin sites on the dextran backbone. To remove
567 any unbound molecules, Ag-scaffolds were filtered through 100 kDa spin columns (Vivaspin6,
568 Sartorius). Ag-scaffolds were frozen in 0.5% BSA and 5% glycerol at −80°C for up to 15 months[21].

569 **Flow cytometry**

570 Cells were stained with antibodies against phenotypic and intracellular markers, then run on a
571 Fortessa (BD) and the data analysed using FlowJo software. For gating strategies **(**see **Figures S7A,**
572 **B, and Figure S8A).** The antibodies used for surface and intracellular marker staining are listed in
573 Key Resouce Table.

574 Cell lines were sorted using a FACSAria flow cytometer (BD, USA) with a 100 µm nozzle.
575 Amplitude was adjusted to optimise droplet break-off, and droplet calibration was performed before
576 each sort using AccuDrop™ beads (BD, USA).

577 **Tetramer staining**

578 Cells were centrifuged at 500 x g for 5 minutes at 4°C, and the supernatant was discarded. The pelleted
579 cells were then resuspended in 5 µL of 1 µM Dasatinib (LC Laboratories, #D3307), antigen tetramers
580 were added, and the cells were incubated for 15 minutes at 37°C in the dark. The cells were washed
581 once with FACS buffer, followed by staining with Near-IR (NiR) viability dye (Invitrogen, #L34976)
582 and additional antibodies for surface staining for surface markers 30 min at 4°C in the dark. Finally,
583 the cells were washed twice with FACS buffer in 200-300 µL of FACS buffer and immediately
584 analysed on a LSRFortessa flow cytometer (BD, USA). Alternatively, the cells were fixed with 50
585 µL of 1% paraformaldehyde for 1-2 hrs (if required), washed twice with FACS buffer, and analysed
586 2-24 hrs later[44]

587 **Proliferation assay**

588 The T cells were resuspended at $1x10^6$ cells/mL in PBS and 0.75µL CellTrace violet/mL of PBS was
589 added and incubated at 37°C for 15 mins. After incubation, the cells were washed 2x and co-cultured
590 with irradiated Jeko-1 target cells at a 1:5 effector-to-target ratio for 6 days. Flow cytometry was used
591 to measure CellTrace Violet dilution, and the results were analysed using FlowJo software (BD,
592 v10.10.0).

593 **Incucyte**

594 The CD19 CAR T cells and the CD19 target cells, Jeko 1 lymphoma cell line modified to express
595 mCherry, resuspended in RPMI supplemented with 10%FBS and 1% PenStrep are seeded at the
596 mentioned effector:target ratio. In Incucyte assays, effector:target ratios were adjusted to the CAR-
597 positive fraction, e.g., 1:1 (10,000 target cells/well: 10,000 CAR^+ T cells adjusted based on the % of
598 CAR T cells present in the final expansion product) on day 0 in a 96-well plate. Plates were incubated
599 at 37°C and 5%CO_2. After 48 hrs of incubation, the supernatant is collected for ELISA, and the wells
600 are rechallenged with 10,000 target cells in 200µL/well. This process is repeated every 48 hrs, to
601 simulate the challenge that the CAR T cells will encounter *in vivo*.

602 The A375 target cells (mCherry-luciferase modified) expressing the target antigen were plated 5000
603 cells/well and incubated overnight, and the CRISPR/Cas9 or Lentivirus-engineered T cells expanded
604 with either IL2/7/15 or Ag-scaffold were added on top at an effector target (E:T) ratio of 4:1 or 1:1
605 adjusted based on the % of TCR^+ T cells present in the final expansion product.

606 **Intracellular staining**

607 The expanded TCR T cells were incubated with the A375 target cells in an effector:target ratio (E:T)
608 of 1:1 for 6 hrs in RPMI media supplemented with αCD107s-PE antibody and GolgiPlug. Negative
609 control was supplemented with media, and the positive control was incubated with a leukocyte-
610 activating cocktail. The T cells were harvested and stained for dead cells and surface markers (αCD3,
611 αCD8) as described previously and the cells were fixed with 4% paraformaldehyde and incubated for
612 30 mins on ice and permeabilised (Invitrogen, #88-8824-00) and stained for intracellular markers
613 (TNFα and IFN-γ) for 30 minutes at 4°C in the dark (Key Resource Table). Finally, the cells were
614 washed twice, resuspended in 200 µL FACS buffer, and analysed on an LSRFortessa.

615 **ELISA**

616 96-well plates are coated with purified mouse anti-human IFN-γ (BD, #551221) resuspended in 0.1
617 M Na_2HPO_4 buffer at (1µg/mL) and coated with 50 µL/well and incubated at 4°C overnight. The
618 coating was removed, and the plates were blocked with blocking buffer (1% BSA in 1xPBS) for 2
619 hrs at RT on a plate shaker at 300 rpm. Blocking buffer was discarded, and samples and standards
620 were incubated at 50 µL/well for 2 hrs at RT at 300 rpm. Following incubation, the plate was washed
621 with PBS-Tween buffer and incubated with 50 µL/well (0.5 µg/mL) of the detecting antibody, Biotin
622 mouse anti-human IFN-γ (BD, #554550), for 1 hr at RT at 300 rpm. The plate was washed with PBS-
623 Tween, and streptavidin-POD conjugate (Merck, #11089153001) was added (50 µL/well) and

624 incubated for 30 mins at RT at 300 rpm. Finally, the plate was washed with PBS-Tween, and 50
625 µL/well TMB (Kem-en-Tec, #4380A) solution was added (50 µL/well). The reaction was stopped by
626 adding 50 µL of H_2SO_4. OD450 was measured. The analysis was done using the Dose-response curve.

627 **Single-cell RNA sequencing**

628 Expanded T cells were stained with multimers and antibodies as previously reported[45,46]. In brief,
629 cells were washed twice with PBS+0.5% BSA. 3µL of the DNA-barcoded pMHC multimer
630 (SLLMWITQC/HLA-A*02:01) was added to the T cells and stained at a final volume of 100 µL for
631 60 min on ice, followed by three washes with PBS+0.5% BSA. Cells were blocked with 2.5µL of
632 Human TruStain FcX Blocking reagent (BioLegend, 422302) for 10 min on ice. TotalSeq-C Human
633 Universal Cocktail V1.0 (BioLegend, 399905) was added and incubated for 10 min, whereafter
634 TotalSeq-C anti-Human Hashtag antibodies (#1-#24) and fluorochrome-conjugated lineage
635 antibodies (LIVE/DEAD™ Fixable Near-IR Dead Cell Stain Kit, BV421-anti-human CD3-BD
636 Biosciences (562877), BV480-anti-human CD8-BD Biosciences(566121), PE-Cy7-anti-CD4-BD
637 Biosciences (560649)) were added, followed by 30 min on ice. Finally, the cells were washed three
638 times prior to acquisition. Cells were sorted into PBS+0.5% BSA and centrifuged at 390g at 4°C for
639 10 min. The cells were resuspended in ~20 µL of the supernatant and loaded into a Chromium
640 Controller and prepared for sequencing as described in the Chromium Next GEM Single Cell 5' v2
641 protocol (CG000330).

642 **Single-cell RNA sequencing analysis**

643 Gene expression (RNA), antibody-derived tag (ADT), and hashtag oligonucleotide (HTO) libraries
644 were sequenced on an Illumina platform at Novogene. Reads were processed using CellRanger multi
645 (cellranger-7.0.0, 10X genomics) with feature references associating barcodes to CITE-seq antibodies
646 and hashing antibodies (reference transcriptome: GRCh38-1.2.0) and analysed using Seurat
647 (V.5.3.0)[47]. Counts for hashtags were normalised and then demultiplexed using HTODemux and only
648 cells identified as singlets were used for downstream analysis.

649 Quality control filtering was applied to remove low-quality cells[48]. Cells expressing <100 and >5,500
650 genes were removed, along with cells with an RNA count of >20,000. Furthermore, cells with >10%
651 mitochondrial reads were removed. Following filtration, a total of 2,292 cells were included in further
652 processing and analysis. The RNA data were normalised, and the effect of the cell cycle was removed
653 by regressing out the S and G2/M scores during data scaling. A set of 2,000 highly variable genes
654 was defined using the FindVariableFeatures function and subsequently utilised for dimensionality

655 reduction via principal component analysis. Cell clustering was performed with the FindNeighbors
656 and FindClusters functions, and Uniform Manifold Approximation and Projection (UMAP) plots
657 were generated using the do_Dimplot function from the SCpubr (V.3.0.0) package[49]. Gene signatures
658 were scored using the AddModuleScore_UCell function from UCell (V.2.12.0) with cytotoxicity
659 being defined by the gene set GZMA, GZMB, GNLY and PRF1, dysfunctionality being defined by
660 the gene set HAVCR2, LAG3, ENTPD1, TCF7-, SLAMF6-, and proliferation being defined by the
661 gene set CCDN3, CDK6, MKI67, PCNA, MCM3, MCM5, MCM7, CLSPN, IL2RA[50]. Violin plots
662 were generated using the VlnPlot function with modifications for adding statistics using the non-
663 parametric Mann-Whitney U test.

664 **Bulk RNA sequencing and differential gene expression analysis**

665 Sorted $CD3^{+}CAR^{+}$ T cells, previously expanded using either Ag-scaffolds or cytokines, were
666 submitted for bulk RNA sequencing at Genewiz®. The resulting raw reads were processed using
667 Trim Galore, and transcript abundances were subsequently quantified with Kallisto Quant[51]. We
668 performed differential gene expression analysis across three donors using DESeq2 in R[52]. Genes were
669 considered differentially expressed if adjusted p-value < 0.05 and Log2 fold change > 2 (upregulated)
670 or < -2 (downregulated). A volcano plot of the results was generated using ggplot2, and a heatmap of
671 selected differentially expressed genes was created with ComplexHeatmap[53].

672 Quantification and statistical analysis

673 For flow cytometry analysis, FlowJo (v10.10.0) was used, and numerical data analysis was performed
674 in GraphPad Prism (v10.5.0). Statistical analysis was performed for normally distributed paired data
675 using ratio-paired T tests. When comparing more than two groups, we used an Ordinary One-Way
676 ANOVA with the Holm-Šídák multiple-comparison correction, unless stated otherwise. Data is
677 presented as individual data points, with mean±SD indicated and *P < 0.05, **P < 0.01, ***P < 0.001,
678 ****P < 0.0001.

679

680 References

681 1. Li, D., Li, X., Zhou, W.-L., Huang, Y., Liang, X., Jiang, L., Yang, X., Sun, J., Li, Z., Han, W.-
682 D., et al. (2019). Genetically engineered T cells for cancer immunotherapy. Signal Transduct
683 Target Ther *4*, 35. https://doi.org/10.1038/s41392-019-0070-9.

684 2. Hong, D.S., Van Tine, B.A., Biswas, S., McAlpine, C., Johnson, M.L., Olszanski, A.J., Clarke,
685 J.M., Araujo, D., Blumenschein, G.R., Kebriaei, P., et al. (2023). Autologous T cell therapy
686 for MAGE-A4+ solid cancers in HLA-A*02+ patients: a phase 1 trial. Nat Med *29*, 104–114.
687 https://doi.org/10.1038/s41591-022-02128-z.

688 3. Chamucero-Millares, J.A., Bernal-Estévez, D.A., and Parra-López, C.A. (2021). Usefulness of
689 IL-21, IL-7, and IL-15 conditioned media for expansion of antigen-specific CD8+ T cells from
690 healthy donor-PBMCs suitable for immunotherapy. Cell Immunol *360*, 104257.
691 https://doi.org/10.1016/j.cellimm.2020.104257.

692 4. Roth, T.L., Puig-Saus, C., Yu, R., Shifrut, E., Carnevale, J., Li, P.J., Hiatt, J., Saco, J.,
693 Krystofinski, P., Li, H., et al. (2018). Reprogramming human T cell function and specificity
694 with non-viral genome targeting. Nature *559*, 405–409. https://doi.org/10.1038/s41586-018-
695 0326-5.

696 5. Eyquem, J., Mansilla-Soto, J., Giavridis, T., van der Stegen, S.J.C., Hamieh, M., Cunanan,
697 K.M., Odak, A., Gönen, M., and Sadelain, M. (2017). Targeting a CAR to the TRAC locus
698 with CRISPR/Cas9 enhances tumour rejection. Nature *543*, 113–117.
699 https://doi.org/10.1038/nature21405.

700 6. Zhang, X., Cheng, C., Sun, W., and Wang, H. (2020). Engineering T Cells Using
701 CRISPR/Cas9 for Cancer Therapy. In, pp. 419–433. https://doi.org/10.1007/978-1-0716-0290-
702 4_23.

703 7. Filosto, S., Vardhanabhuti, S., Canales, M.A., Poiré, X., Lekakis, L.J., de Vos, S., Portell, C.A.,
704 Wang, Z., To, C., Schupp, M., et al. (2024). Product Attributes of CAR T-cell Therapy
705 Differentially Associate with Efficacy and Toxicity in Second-line Large B-cell Lymphoma
706 (ZUMA-7). Blood Cancer Discov *5*, 21–33. https://doi.org/10.1158/2643-3230.BCD-23-0112.

707 8. Garfall, A.L., Dancy, E.K., Cohen, A.D., Hwang, W.-T., Fraietta, J.A., Davis, M.M., Levine,
708 B.L., Siegel, D.L., Stadtmauer, E.A., Vogl, D.T., et al. (2019). T-cell phenotypes associated
709 with effective CAR T-cell therapy in postinduction vs relapsed multiple myeloma. Blood Adv
710 *3*, 2812–2815. https://doi.org/10.1182/bloodadvances.2019000600.

711 9. Cappell, K.M., and Kochenderfer, J.N. (2023). Long-term outcomes following CAR T cell
712 therapy: what we know so far. Nat Rev Clin Oncol *20*, 359–371.
713 https://doi.org/10.1038/s41571-023-00754-1.

714 10. Deng, Q., Han, G., Puebla-Osorio, N., Ma, M.C.J., Strati, P., Chasen, B., Dai, E., Dang, M.,
715 Jain, N., Yang, H., et al. (2020). Characteristics of anti-CD19 CAR T cell infusion products
716 associated with efficacy and toxicity in patients with large B cell lymphomas. Nat Med *26*,
717 1878–1887. https://doi.org/10.1038/s41591-020-1061-7.

718 11. Majzner, R.G., and Mackall, C.L. (2019). Clinical lessons learned from the first leg of the CAR
719 T cell journey. Nat Med *25*, 1341–1355. https://doi.org/10.1038/s41591-019-0564-6.

720 12. Tang, L., Zhang, Y., Hu, Y., and Mei, H. (2021). T Cell Exhaustion and CAR-T
721 Immunotherapy in Hematological Malignancies. Biomed Res Int *2021*, 1–8.
722 https://doi.org/10.1155/2021/6616391.

723 13. Kalamasz, D., Long, S.A., Taniguchi, R., Buckner, J.H., Berenson, R.J., and Bonyhadi, M.
724 (2004). Optimization of Human T-Cell Expansion Ex Vivo Using Magnetic Beads Conjugated
725 with Anti-CD3 and Anti-CD28 Antibodies. Journal of Immunotherapy *27*, 405–418.
726 https://doi.org/10.1097/00002371-200409000-00010.

727 14. Kagoya, Y., Nakatsugawa, M., Ochi, T., Cen, Y., Guo, T., Anczurowski, M., Saso, K., Butler,
728 M.O., and Hirano, N. (2017). Transient stimulation expands superior antitumor T cells for
729 adoptive therapy. JCI Insight *2*. https://doi.org/10.1172/jci.insight.89580.

730 15. Mo, F., Yu, Z., Li, P., Oh, J., Spolski, R., Zhao, L., Glassman, C.R., Yamamoto, T.N., Chen,
731 Y., Golebiowski, F.M., et al. (2021). An engineered IL-2 partial agonist promotes CD8+ T cell
732 stemness. Nature *597*, 544–548. https://doi.org/10.1038/s41586-021-03861-0.

733 16. Li, Y., Cong, Y., Jia, M., He, Q., Zhong, H., Zhao, Y., Li, H., Yan, M., You, J., Liu, J., et al.
734 (2021). Targeting IL-21 to tumor-reactive T cells enhances memory T cell responses and anti-
735 PD-1 antibody therapy. Nat Commun *12*, 951. https://doi.org/10.1038/s41467-021-21241-0.

736 17. Santegoets, S.J.A.M., Turksma, A.W., Suhoski, M.M., Stam, A.G.M., Albelda, S.M.,
737 Hooijberg, E., Scheper, R.J., van den Eertwegh, A.J.M., Gerritsen, W.R., Powell, D.J., et al.
738 (2013). IL-21 promotes the expansion of CD27+ CD28+ tumor infiltrating lymphocytes with
739 high cytotoxic potential and low collateral expansion of regulatory T cells. J Transl Med *11*,
740 37. https://doi.org/10.1186/1479-5876-11-37.

741 18. Isser, A., Livingston, N.K., and Schneck, J.P. (2021). Biomaterials to enhance antigen-specific
742 T cell expansion for cancer immunotherapy. Biomaterials *268*, 120584.
743 https://doi.org/10.1016/j.biomaterials.2020.120584.

744 19. Rhodes, K.R., and Green, J.J. (2018). Nanoscale artificial antigen presenting cells for cancer
745 immunotherapy. Mol Immunol *98*, 13–18. https://doi.org/10.1016/j.molimm.2018.02.016.

746 20. Tvingsholm, S.A., Frej, M.S., Rafa, V.M., Hansen, U.K., Ormhøj, M., Tyron, A., Jensen,
747 A.W.P., Kadivar, M., Bentzen, A.K., Munk, K.K., et al. (2023). TCR-engaging scaffolds
748 selectively expand antigen-specific T-cells with a favorable phenotype for adoptive cell
749 therapy. J Immunother Cancer *11*, e006847. https://doi.org/10.1136/jitc-2023-006847.

750 21. Tvingsholm, S.A., Frej, M.S., Rafa, V.M., Hansen, U.K., Ormhøj, M., Tyron, A., Jensen,
751 A.W.P., Kadivar, M., Bentzen, A.K., Munk, K.K., et al. TCR-engaging scaffolds selectively
752 expand antigen-specific T-cells with a favorable phenotype for adoptive cell therapy. *11*,
753 e006847. https://doi.org/10.1136/jitc-2023-006847.

754 22. Hendriks, J., Xiao, Y., and Borst, J. (2003). CD27 Promotes Survival of Activated T Cells and
755 Complements CD28 in Generation and Establishment of the Effector T Cell Pool. J Exp Med
756 *198*, 1369–1380. https://doi.org/10.1084/jem.20030916.

757 23. Palmer, D.C., Guittard, G.C., Franco, Z., Crompton, J.G., Eil, R.L., Patel, S.J., Ji, Y., Van
758 Panhuys, N., Klebanoff, C.A., Sukumar, M., et al. (2015). Cish actively silences TCR signaling
759 in CD8+ T cells to maintain tumor tolerance. Journal of Experimental Medicine *212*, 2095–
760 2113. https://doi.org/10.1084/jem.20150304.

761 24. Schlabach, M.R., Lin, S., Collester, Z.R., Wrocklage, C., Shenker, S., Calnan, C., Xu, T.,
762 Gannon, H.S., Williams, L.J., Thompson, F., et al. (2023). Rational design of a SOCS1-edited
763 tumor-infiltrating lymphocyte therapy using CRISPR/Cas9 screens. Journal of Clinical
764 Investigation *133*. https://doi.org/10.1172/JCI163096.

765 25. Madura, F., Rizkallah, P.J., Holland, C.J., Fuller, A., Bulek, A., Godkin, A.J., Schauenburg,
766 A.J., Cole, D.K., and Sewell, A.K. (2015). Structural basis for ineffective T-cell responses to
767 MHC anchor residue-improved "heteroclitic" peptides. Eur J Immunol *45*, 584–591.
768 https://doi.org/10.1002/eji.201445114.

769 26. Smith, A.R., Alonso, J.A., Ayres, C.M., Singh, N.K., Hellman, L.M., and Baker, B.M. (2021).
770 Structurally silent peptide anchor modifications allosterically modulate T cell recognition in a
771 receptor-dependent manner. Proceedings of the National Academy of Sciences *118*.
772 https://doi.org/10.1073/pnas.2018125118.

773 27. Murata, K., Nakatsugawa, M., Rahman, M.A., Nguyen, L.T., Millar, D.G., Mulder, D.T.,
774 Sugata, K., Saijo, H., Matsunaga, Y., Kagoya, Y., et al. (2020). Landscape mapping of shared
775 antigenic epitopes and their cognate TCRs of tumor-infiltrating T lymphocytes in melanoma.
776 Elife *9*. https://doi.org/10.7554/eLife.53244.

777 28. Mizukami, A., and Swiech, K. (2020). Platforms for Clinical-Grade CAR-T Cell Expansion.
778 In, pp. 139–150. https://doi.org/10.1007/978-1-0716-0146-4_10.

779 29. Rushworth, D., Jena, B., Olivares, S., Maiti, S., Briggs, N., Somanchi, S., Dai, J., Lee, D., and
780 Cooper, L.J.N. (2014). Universal artificial antigen presenting cells to selectively propagate t
781 cells expressing chimeric antigen receptor independent of specificity. Journal of
782 Immunotherapy *37*, 204–213. https://doi.org/10.1097/CJI.0000000000000032.

783 30. Schmidts, A., Marsh, L.C., Srivastava, A.A., Bouffard, A.A., Boroughs, A.C., Scarfò, I.,
784 Larson, R.C., Bedoya, F., Choi, B.D., Frigault, M.J., et al. (2020). Cell-based artificial APC
785 resistant to lentiviral transduction for efficient generation of CAR-T cells from various cell
786 sources. J Immunother Cancer *8*, e000990. https://doi.org/10.1136/jitc-2020-000990.

787 31. Niu, H., Zhao, P., and Sun, W. (2023). Biomaterials for chimeric antigen receptor T cell
788 engineering. Acta Biomater *166*, 1–13. https://doi.org/10.1016/j.actbio.2023.04.043.

789 32. Householder, K.D., Xiang, X., Jude, K.M., Deng, A., Obenaus, M., Zhao, Y., Wilson, S.C.,
790 Chen, X., Wang, N., and Garcia, K.C. (2025). De novo design and structure of a peptide–
791 centric TCR mimic binding module. Science (1979) *389*, 375–379.
792 https://doi.org/10.1126/science.adv3813.

793 33. Johansen, K.H., Wolff, D.S., Scapolo, B., Fernández-Quintero, M.L., Risager Christensen, C.,
794 Loeffler, J.R., Rivera-de-Torre, E., Overath, M.D., Kjærgaard Munk, K., Morell, O., et al.
795 (2025). De novo-designed pMHC binders facilitate T cell–mediated cytotoxicity toward cancer
796 cells. Science (1979) *389*, 380–385. https://doi.org/10.1126/science.adv0422.

797 34. Liu, B., Greenwood, N.F., Bonzanini, J.E., Motmaen, A., Meyerberg, J., Dao, T., Xiang, X.,
798 Ault, R., Sharp, J., Wang, C., et al. (2025). Design of high-specificity binders for peptide–
799 MHC-I complexes. Science (1979) *389*, 386–391. https://doi.org/10.1126/science.adv0185.

800 35. Powell, D.J., Dudley, M.E., Robbins, P.F., and Rosenberg, S.A. (2005). Transition of late-
801 stage effector T cells to CD27+ CD28+ tumor-reactive effector memory T cells in humans

802 after adoptive cell transfer therapy. Blood *105*, 241–250. https://doi.org/10.1182/blood-2004-
803 06-2482.

804 36. Wherry, E.J., and Kurachi, M. (2015). Molecular and cellular insights into T cell exhaustion.
805 Nat Rev Immunol *15*, 486–499. https://doi.org/10.1038/nri3862.

806 37. Wherry, E.J. (2011). T cell exhaustion. Nat Immunol *12*, 492–499.
807 https://doi.org/10.1038/ni.2035.

808 38. Shy, B.R., Vykunta, V.S., Ha, A., Talbot, A., Roth, T.L., Nguyen, D.N., Pfeifer, W.G., Chen,
809 Y.Y., Blaeschke, F., Shifrut, E., et al. (2023). High-yield genome engineering in primary cells
810 using a hybrid ssDNA repair template and small-molecule cocktails. Nat Biotechnol *41*, 521–
811 531. https://doi.org/10.1038/s41587-022-01418-8.

812 39. Rohland, N., and Reich, D. (2012). Cost-effective, high-throughput DNA sequencing libraries
813 for multiplexed target capture. Genome Res *22*, 939–946.
814 https://doi.org/10.1101/GR.128124.111.

815 40. Schober, K., Müller, T.R., Gökmen, F., Grassmann, S., Effenberger, M., Poltorak, M.,
816 Stemberger, C., Schumann, K., Roth, T.L., Marson, A., et al. (2019). Orthotopic replacement
817 of T-cell receptor α- and β-chains with preservation of near-physiological T-cell function. Nat
818 Biomed Eng *3*, 974–984. https://doi.org/10.1038/s41551-019-0409-0.

819 41. Dull, T., Zufferey, R., Kelly, M., Mandel, R.J., Nguyen, M., Trono, D., and Naldini, L. (1998).
820 A third-generation lentivirus vector with a conditional packaging system. J Virol *72*, 8463–
821 8471. https://doi.org/10.1128/JVI.72.11.8463-8471.1998.

822 42. Saini, S.K., Tamhane, T., Anjanappa, R., Saikia, A., Ramskov, S., Donia, M., Svane, I.M.,
823 Jakobsen, S.N., Garcia-Alai, M., Zacharias, M., et al. (2019). Empty peptide-receptive MHC
824 class I molecules for efficient detection of antigen-specific T cells. Sci Immunol *4*.
825 https://doi.org/10.1126/sciimmunol.aau9039.

826 43. Rodenko, B., Toebes, M., Hadrup, S.R., van Esch, W.J.E., Molenaar, A.M., Schumacher,
827 T.N.M., and Ovaa, H. (2006). Generation of peptide–MHC class I complexes through UV-
828 mediated ligand exchange. Nat Protoc *1*, 1120–1132. https://doi.org/10.1038/nprot.2006.121.

829 44. Friis, R.U.W., Ormhøj, M., Krüger-Jensen, C.S., Pardo, C.R., Halldórsdóttir, H.R., Barden,
830 M., Kristensen, N.P., Ramanathan, K., Hansen, M.R., Abken, H., et al. (2025). Development

831 of antigen multimers for detection and evaluation of CAR T cells. Cancer Immunology,
832 Immunotherapy *74*, 344. https://doi.org/10.1007/s00262-025-04134-9.

833 45. Povlsen, H.R., Bentzen, A.K., Kadivar, M., Jessen, L.E., Hadrup, S.R., and Nielsen, M. (2023).
834 Improved T cell receptor antigen pairing through data-driven filtering of sequencing
835 information from single cells. Elife *12*. https://doi.org/10.7554/eLife.81810.

836 46. Kristensen, N.P., Heeke, C., Tvingsholm, S.A., Borch, A., Draghi, A., Crowther, M.D., Carri,
837 I., Munk, K.K., Holm, J.S., Bjerregaard, A.M., et al. (2022). Neoantigen-reactive CD8+ T cells
838 affect clinical outcome of adoptive cell therapy with tumor-infiltrating lymphocytes in
839 melanoma. Journal of Clinical Investigation *132*. https://doi.org/10.1172/JCI150535.

840 47. Hao, Y., Stuart, T., Kowalski, M.H., Choudhary, S., Hoffman, P., Hartman, A., Srivastava, A.,
841 Molla, G., Madad, S., Fernandez-Granda, C., et al. (2024). Dictionary learning for integrative,
842 multimodal and scalable single-cell analysis. Nat Biotechnol *42*, 293–304.
843 https://doi.org/10.1038/s41587-023-01767-y.

844 48. Hayakawa, Y., and Ozaki, H. (2025). A practical guide for single-cell transcriptome data
845 analysis in neuroscience. Neurosci Res *214*, 9–15.
846 https://doi.org/10.1016/j.neures.2025.03.006.

847 49. Blanco-Carmona, E. (2022). Generating publication ready visualizations for Single Cell
848 transcriptomics using SCpubr. Preprint, https://doi.org/10.1101/2022.02.28.482303
849 https://doi.org/10.1101/2022.02.28.482303.

850 50. Andreatta, M., and Carmona, S.J. (2021). UCell: Robust and scalable single-cell gene signature
851 scoring. Comput Struct Biotechnol J *19*, 3796–3798.
852 https://doi.org/10.1016/j.csbj.2021.06.043.

853 51. Bray, N.L., Pimentel, H., Melsted, P., and Pachter, L. (2016). Near-optimal probabilistic RNA-
854 seq quantification. Nat Biotechnol *34*, 525–527. https://doi.org/10.1038/nbt.3519.

855 52. Love, M.I., Huber, W., and Anders, S. (2014). Moderated estimation of fold change and
856 dispersion for RNA-seq data with DESeq2. Genome Biol *15*. https://doi.org/10.1186/s13059-
857 014-0550-8.

858 53. Gu, Z., Eils, R., and Schlesner, M. (2016). Complex heatmaps reveal patterns and correlations
859 in multidimensional genomic data. Bioinformatics *32*, 2847–2849.
860 https://doi.org/10.1093/bioinformatics/btw313.